

Theoretical Simulation of Resonant Inelastic X-Ray Scattering In Transition Metal Oxides

Siobhán Grayson
Senior Sophister Physics



Supervisor: Dr C. McGuinness

Department of Physics
Trinity College Dublin

January 2012

Abstract

Metal L -edge 2p-3d resonant inelastic x-ray scattering (RIXS) spectra of TiO_2 was simulated and compared with previously obtained experimental RIXS spectra. This was done by applying an atomic multiplet model to the $2p^63d^N2p^53d^{N+1}$ transition in tetragonal symmetry (D_{4h}) and allowing for solid state effects such as crystal field interactions with the oxygen ligands of the metal ion to be taken into account. X-ray absorption spectroscopy (XAS) calculations were computed for Ti^{4+} and Ti^{3+} configurations in both octahedral and tetragonal symmetries. These calculations included not only crystal field interactions but also charge-transfer between the metal ion and surrounding ligands. Ti^{4+} simulations were compared against a rutile TiO_2 Ti L -edge XAS spectrum. Ti^{3+} simulations were compared against a sputtered rutile TiO_2 Ti L -edge XAS spectrum.

Acknowledgements

I would like to express my thanks and sincere gratitude to my supervisor, Dr. Cormac McGuinness, for his kind support, advice and encouragement. For always making the time to answer questions, and for being so friendly and approachable. Turning to Cormac for advice was never a problem and a solution was always found.

I would also like to thank Declan Cockburn, Martin Duignan, and Stephan Callaghan, whom were never too busy to offer their advice. In particular, my sincere thanks to Declan for sharing not only his experimental rutile TiO_2 XAS spectrum but for his immense wisdom of Origin and for advising me on how best to present my simulations. Thanks to Stephan, whom not only shared his sputtered rutile TiO_2 XAS spectrum but also offered me great support when times got tough.

I will miss researching with the TCD X-Ray Group, it's been a privilege getting to know you all.



Contents

1	Introduction	1
1.1	X-Ray Absorption Spectroscopy	2
1.2	X-Ray Emission Spectroscopy	3
1.3	Resonant Inelastic X-Ray Spectroscopy	4
1.4	Titanium Dioxide	5
2	Theoretical Background	6
2.1	Atomic Multiplet Calculations	7
2.2	Ligand Field Multiplet Theory	10
2.3	Crystal Field Theory	10
2.4	Charge Transfer Multiplet Theory	13
2.5	Resonant Inelastic X-Ray Scattering	14
2.6	Spectroscopic Simulation Software	14
3	Computational Method	15
3.1	Method for Simulating XAS	15
3.2	Method for Simulating RXIS	17
4	Results and Discussion	18
4.1	Simulated Ti^{4+} 2p XAS	18
4.1.1	Octahedral Symmetry	19
4.1.2	Tetragonal Symmetry	21
4.2	Simulated Ti^{3+} 2p-3d XAS	24
4.2.1	Octahedral Symmetry	24
4.2.2	Tetragonal Symmetry	26
4.3	Ti^{3+} 2p-3d RIXS	28
5	Conclusions	29
	Appendices	30
5.1	Appendix A	30
5.1.1	The Dipole Selection Rules	30

5.1.2	The Hartree-Fock Method	30
5.1.3	Lamor Formula	30
5.2	Appendix B	31
5.2.1	Broadening Parameters	31
5.3	Appendix C	35
5.3.1	Varying the Crystal Field	35
5.3.2	Crystal Field Parameters	38
5.3.3	RIXS Simulation: Incident Energy Vs Emitted Energy	40
	Bibliography	40

Chapter 1

Introduction

Resonant inelastic x-ray scattering (RIXS) belongs to a family of experimental techniques known as spectroscopy. Spectroscopy is the study of the interaction between matter and radiated energy. It is a broad field encompassing many sub-disciplines, each with numerous implementations of specific spectroscopic techniques. These techniques are a powerful tool for probing the electronic structure of materials, which characterise most of a material's relevant attributes. Due to the recent advent of high-brilliance synchrotron radiation sources [1], the development of one field in particular, known as core level spectroscopy, has been remarkable. Core level spectroscopy is used to study valence electron states (VES), the states responsible for the bonding in molecules and solids [2].

Such photon energies belong mainly to the soft x-ray region (between 100 eV and 3 keV). The VES are detected with the core electron or (core hole) state as a probe, where the core hole is defined as the absence of a core electron in a core level. This process is essentially the photoelectric effect and forms the basis of three of the most important spectroscopic techniques; x-ray photo-emission spectroscopy (XPS), x-ray absorption spectroscopy (XAS), and x-ray emission spectroscopy (XES) [3]. Due to these advances, interest has grown in establishing an ideal theoretical model from which spectra can be reliably simulated. Such models also allow further insight into the processes which occur during spectroscopic measurements.

This report is primarily concerned with the theoretical simulation of XAS and RIXS. Simulations will be carried out using two programs, CTM4XAS 5.2 and CTM4RIXS. The transition metal (TM) compound, titanium dioxide (TiO_2), will be the subject of each investigation and will be compared against actual XAS and RIXS data of TiO_2 . For the remainder of this introduction, one will explain the processes of XAS, XES, and RIXS, including a brief description of TiO_2 . This is followed by a discussion, in chapter 2, on the theoretical methods behind the spectroscopic simulations computed by CTM4XAS 5.2 and CTM4RIXS. Chapter 3. will describe the methods used to obtain simulated spectra, after which, in chapter 4, one will present the simulated results obtained from CTM4XAS 5.2 and CTM4RIXS, drawing comparison to experimental data.

1.1 X-Ray Absorption Spectroscopy

In x-ray absorption spectroscopy, the absorption of x-rays by a sample is measured [3]. For instance, when an experimental sample is illuminated by synchrotron radiation, transitions of core electrons to the conduction band (CB) (or continuum) take place as they absorb energy from the incident radiation.

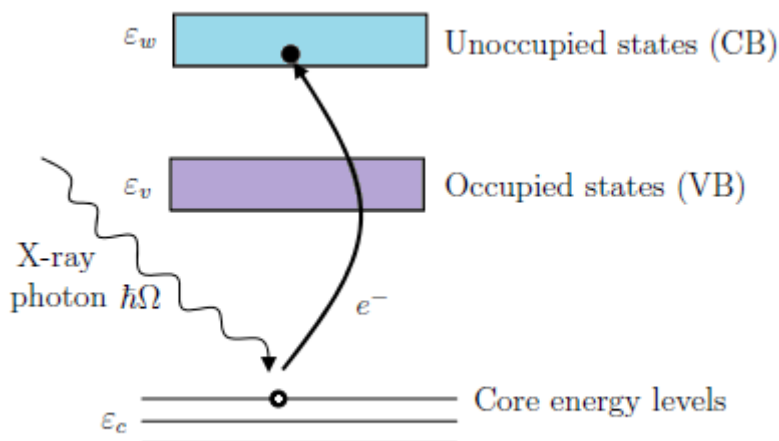


Figure 1.1: Schematic diagram of x-ray absorption.

In Figure 1.1, a core electron has been excited from a core energy level (with binding energy equal to ε_c , to an empty or unoccupied state with energy ε_w . Thus, the energy of the incident photon $\hbar\Omega$ is such that:

$$\hbar\Omega = \varepsilon_w - \varepsilon_c \quad (1.1)$$

This means that as light of intensity I_0 is exposed to a sample, it is partially absorbed resulting in an attenuated beam of intensity I . The amount of absorption is proportional to the thickness (x) of the sample as well as the linear absorption coefficient, μ which depends on the type of atoms and the density ρ of the material.

$$\ln I_0/I = \mu x \quad (1.2)$$

Plotting μ against the excitation energy will show features known as absorption edges where the excitation energy corresponds to the difference between a core-hole binding energy and an unoccupied state¹. In other words, the photon energy is equal to the binding energy of electrons in the shells (s, p, d, f,...) of the absorbing element.

¹An XAS spectrum is also dependant upon the dipole selection rules. Refer to Appendix A, Section 5.1.1.

The absorption edges are labelled in the order of increasing energy:

$$K, L_1, L_2, L_3, M_1, \dots$$

where the K edge relates to a 1s core level and where the $L_{2,3}$ edges relate to a 2p core level binding energy [3].

Thus, by knowing the energy of the incident X-ray, one can determine the energy separation between the core level and the unoccupied level. This is how XAS probe the local partial densities of unoccupied electronic states. Furthermore, because each element has a characteristic binding energy for a certain core level, XAS is also an element specific technique [4].

1.2 X-Ray Emission Spectroscopy

In XAS, the incident x-ray causes a core electron to move to an unoccupied state. This electron leaves behind what is known as a core hole. X-ray emission spectroscopy detects the emitted photon, which is created when an electron from either the valance or conduction band refills the core hole created in XAS, as in Figure 1.2.

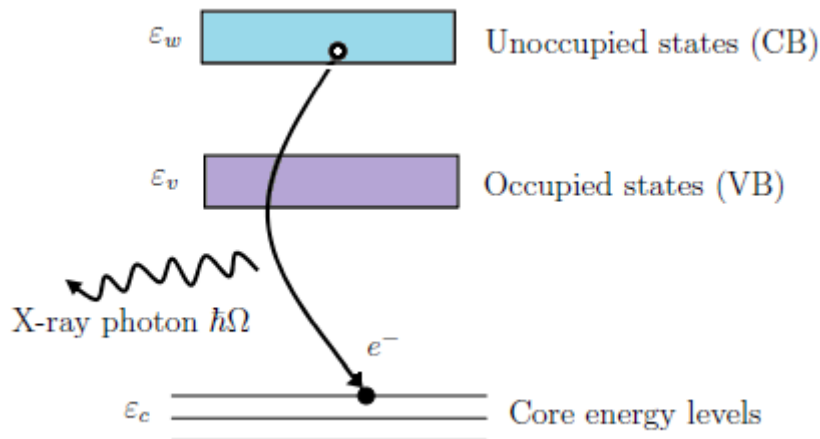


Figure 1.2: Schematic diagram of x-ray emission.

The energy of this emitted photon is equivalent to the energy difference between the core level and valence level. This is how XES probe the local partial densities of occupied electronic states. Thus, XES is a second-order optical process, where first a core electron is excited by an incident x-ray photon (XAS) followed by the excited state decaying by emitting an x-ray photon to fill the core hole [3]. As such, this makes XES a photon in, photon out process, where no charging effect occurs, which makes this process favourable to measure both conducting and insulating samples [4].

Moreover, depending on the excitation energy, XES can be categorized even further. When the core electron is excited to the high-energy continuum well above the absorption threshold², it is called non-resonant x-ray emission spectroscopy (NXES) [3]. NXES is generally used to find out information about the partial density of occupied states.

If the core electron is resonantly excited to the absorption threshold by the incident photon (as in the process of XAS), the resulting emission spectrum depends strongly on the incident-photon energy Ω , and the process is referred to as resonant soft x-ray emission (RSXE). RSXE can either be resonant elastic x-ray scattering (RXES), or resonant inelastic x-ray scattering (RIXS).

1.3 Resonant Inelastic X-Ray Spectroscopy

If the atomic state relaxes fully by the emission of a single photon of energy ω after having been excited by the incident photon of energy Ω (as in Figure 1.2), then $\omega = \Omega$ and one says the photon was elastically scattered. If the atomic state relaxes fully by emitting a photon of energy $\omega \neq \Omega$, due to a secondary process, then one says the photon was inelastically scattered [5], as can be seen in Figure 1.3.

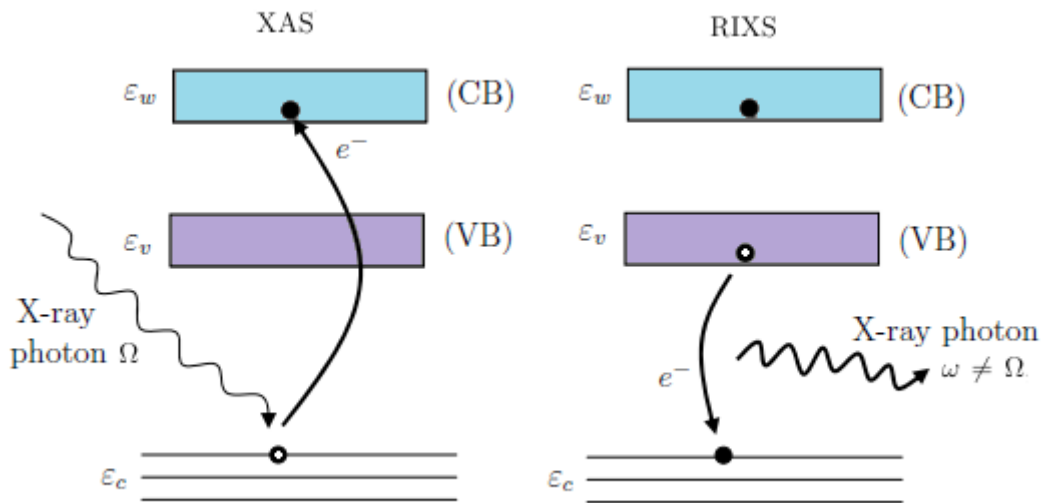


Figure 1.3: Schematic diagram of resonant inelastic x-ray scattering.

Elastic scattering is useful as a monitor of incident light and hence for calibration. However, the inelastic scattering and the associated intermediate processes are generally of more interest [5]. RIXS is useful for probing low energy excitations, such as d-d and charge transfer excitations [4].

²This is the case for x-ray photoemission spectroscopy (XPS)

Since RIXS includes absorption as an excitation process and further includes information on radiative decay, the information given by it is much greater than that given by the first-order optical processes of x-ray absorption or photo-emission. It provides bulk-sensitive and site-selective information. However, the intensity of the signal in a second-order optical process is much weaker than that of a first-order optical process because the efficiency of x-ray emission is quite low. As a result, state-of-the-art experimental instrumentation is needed to obtain precise experimental data [1].

1.4 Titanium Dioxide

Titanium dioxide (TiO_2) is a transition metal compound that occurs in nature as the minerals rutile, anatase and brookite. Rutile is one of the simplest and most common structural types adopted by metal oxides and is the form that will be used throughout this report. It contains six coordinated titanium within a tetragonal lattice, which can be thought of as a cubic lattice stretched along one of its lattice vectors. TiO_2 has many applications such as a photo-catalyst, sunscreen, electronic data storage (a memristor), and pigment. Figure 1.4 depicts the structure of the rutile TiO_2 unit cell from three different perspectives.

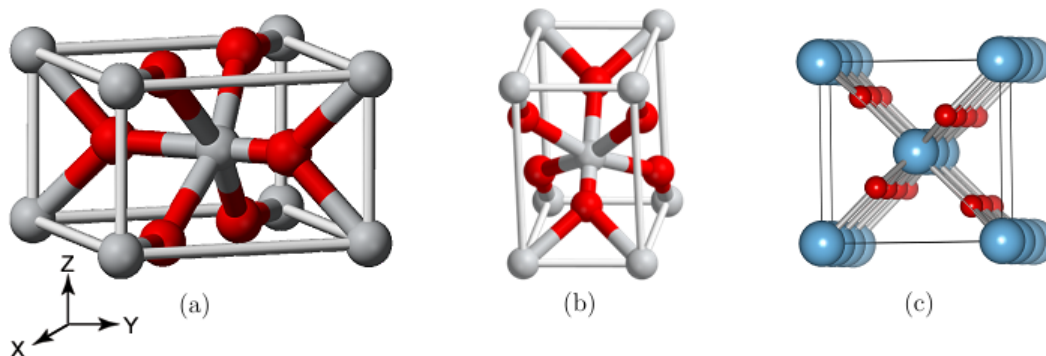


Figure 1.4: (a) TiO_2 rutile unit cell where stretched apex lies \sim along the y-axis. (b) TiO_2 rutile unit cell oriented such that the stretched apex lies in a vertical direction \sim along the z-axis. (c) TiO_2 rutile unit cell as viewed when stretched apex lies \sim along the x-axis.

Chapter 2

Theoretical Background

In XAS, a core electron is excited to an empty state generating a core hole, for instance, a 2p core hole is created in the Ti^{4+} XAS transition $2p^63d^0$ to $2p^53d^1$. Thus, the final state of the XAS process contains a partly filled core state ($2p^5$) and a partly filled valence state ($3d^1$). A strong overlap between the 2p-hole and 3d-hole radial wave functions split the XAS final states. These XAS final states created through splitting are known as atomic multiplets. This overlapping of wave-functions also exists in the ground state, but does not play an effective role here since the core states in the XAS ground state are filled. This is why a single particle description is not capable of calculating the correct density-of-states (DOS) for XAS of transition metal $L_{2,3}$ edges.

Atomic multiplet calculations, where only the interactions within the absorbing atom are considered, without any influence from the surrounding atoms will be described first. However, in the case of 3d TM ions, atomic multiplet theory considered by it's self, will not adequately simulate XAS spectra as the effects of neighbouring ions in the 3d states are too large. It turns out that both the symmetry effects and the charge-transfer effects of the neighbours must be included explicitly. Thus, it is necessary to introduce the ligand field multiplet model, which takes care of all the symmetry effects via the crystal field effect. Followed by a description of charge transfer multiplet theory which allows the use of more than one configuration so that ligand bonds can be accounted for [3]. Altogether, these theories are used to theoretically calculate experimental spectra and to facilitate the analysis of such data [4].

2.1 Atomic Multiplet Calculations

Atomic multiplet calculations are based upon Hartree-Fock approximations¹ and atomic multiplet theory [4]. Atomic multiplet theory is the description of atomic structure using quantum mechanics [3]. The reason for employing quantum mechanics is due to the nature of the elements within an atomic structure. In the classical description of an electron orbiting a nucleus, the electron will accelerate and radiate energy. As a result, the electron should eventually lose its energy and spiral into the nucleus, making atoms quite unstable. However, this is not what is observed. Instead, atoms are stable on time-scales much longer than predicted by the classical Larmor formula² [6].

The starting point is the Schrödinger equation of a single electron in an atom:

$$\hat{H}\Psi = \hat{E}\Psi \quad (2.1)$$

where \hat{H} is the Hamiltonian operator equal to:

$$\hat{H} = \frac{-\hbar^2}{2m}\nabla^2 - \frac{Ze^2}{\vec{r}} \quad (2.2)$$

The solutions of this equation are the atomic orbitals as defined by their quantum numbers n (principle), l (azimuthal), and m (magnetic). In atoms which are not influenced by their surroundings and where more than one electron is present, there are two additional terms in the atomic Hamiltonian:

1. The electron-electron repulsion (H_{ee}) and
2. The spin-orbit coupling of each electron ($H_{\ell s}$).

The total Hamiltonian is then give by:

$$H_{ATOM} = \underbrace{\sum_{i=1}^N \frac{\vec{p}_i^2}{2m}}_1 + \underbrace{\sum_{i=1}^N \frac{-Ze}{\vec{r}_i}}_2 + \underbrace{\sum_{pairs} \frac{e^2}{\vec{r}_{ij}}}_3 + \underbrace{\sum_{i=1}^N \zeta(\vec{r}_i) l_i \times s_i}_4 \quad (2.3)$$

The first term represents the kinetic energy of the electrons, the second term represents the electrostatic interaction of the electrons with the nucleus, the third term represents the electron-electron repulsion (H_{ee}), and the fourth term stands for the spin-orbit coupling ($H_{\ell s}$) of each electron. The kinetic energy and the interaction with the nucleus are the same for all electrons in a given atomic configuration [3]. Thus, the first two terms define the average energy of the configuration (H_{avg}) and do not contribute to the multiplet

¹Refer to Appendix A, Section 5.1.2.

²Refer to Appendix A, Section 5.1.3.

splitting. The remaining two terms (H_{ee} and H_{ls}) define the relative energy of the different terms within the configuration and contribute to the multiplet splitting [4].

However, H_{ee} is too large to be treated as a perturbation and creates difficulty in solving the Schrödinger equation. Thus, the central field approximation is applied [3]. For an electron pair where one electron is close to the nucleus and the other is far away, one imagines that the radial component is the dominant one. This leads to the assumption that, on average, a large fraction of the electrostatic electron-electron interaction can be considered radial, in other words, represented by a central field. While the remaining non-central part is small enough to be treated as a perturbation [7]. As such, the spherical average of the electron-electron interaction $\langle H_{ee} \rangle$ is separated from the non-spherical part and added to H_{avg} to form the average energy of the configuration. Thus, H_{avg} does not contribute to the multiplet splittings [8]. The modified electron-electron Hamiltonian H'_{ee} where the spherical average has been subtracted is now small enough to be treated as a perturbation [3].

$$H'_{ee} = H_{ee} - \langle H_{ee} \rangle \quad (2.4)$$

$$= \sum_{pairs} \frac{e^2}{r_{ij}} \langle \sum_{pairs} \frac{e^2}{r_{ij}} \rangle \quad (2.5)$$

Therefore, H'_{ee} and H_{ls} define the effective Hamiltonian responsible for the multiplet splitting that determines the energy of the different terms in the configuration [4].

Atomic spectral lines correspond to transitions between quantum states of an atom. These states are labelled by a set of quantum numbers summarized in what are known as term symbols [9]. Thus, term symbols are an abbreviated description of the angular momentum quantum numbers in a multi-electron atom [10]. They allow someone to find out the three relevant quantum numbers as well as to determine the energy and symmetry associated with a certain configuration. For instance, a 2p electron with $L = 1$, $S = 1/2$, and $J = 1/2, 3/2$, the term symbols are written as $^2P_{1/2}$ and $^2P_{3/2}$, where spin-orbit coupling is important. These two terms are seen in the experimental 2p XAS of a transition metal as the L_2 and L_3 peaks [4].

To determine the relative energies of different terms derived from the formula $^{2S+1}X_J$, one calculates the matrix elements of these states with the effective Hamiltonian:

$$H_{ee} + H_{lz} = \sum_{pairs} \frac{e^2}{r_{ij}} + \sum_N \zeta(\vec{r}_i) \ell_i \cdot s_i \quad (2.6)$$

The general formula to calculate the matrix elements of two-electron wave-functions can be written as [3]:

$$\langle {}^{2S+1}L_J | \frac{e^2}{r_{12}} | {}^{2S+1}L_J \rangle = \sum_k f_k F^k + \sum_k g_k G^k \quad (2.7)$$

To obtain this equation, the radial parts F^k and G^k have been separated using the Wigner-Eckhart theorem³ and the Hamiltonian $1/r_{12}$ has been expanded by Legendre polynomials. For three or more electrons, it can be shown that the three-electron wave-function can be built from the two-electron wave functions with the use of so-called coefficients of fractional parentage [3].

F^k and G^k in equation (2.7) are the Slater-Condon parameters for the direct Coulomb repulsion and the Coulomb exchange interaction, respectively. G^k values have an approximately constant ratio with respect to the F^k values [3]. Within the program CTM4XAS 5.2, they are incorporated via the ‘Slater Integral Reduction (%)’ as F_{dd} , F_{pd} , and G_{pd} . F_{dd} and F_{pd} represent the radial parts of the 2p-3d Coulomb multi-pole interactions whilst G_{pd} represents the exchange multi-pole interactions [8]. The default setting, 1, for each of these parameters within CTM4XAS 5.2, is equal to 80% of their calculated values [14]. This correction is to account for intra-atomic configuration interaction [8], or in other words, the overestimation of the electron-electron repulsion in the atomic calculation [3].

For tetravalent titanium (Ti^{4+}), a $3d^0 \rightarrow 2p^5 3d^1$ transition occurs at the $L_{2,3}$ edge [14]. The initial state is given by the matrix element $\langle 3d^1 | H_{ATOM} | 3d^1 \rangle$ and the final state by the matrix element $\langle 2p^5 3d^1 | H_{ATOM} | 2p^5 3d^1 \rangle$. The final state atomic energy matrix of 2p3d, consists of terms related to the two-electron Slater integrals ($H_{ELECTRO}$), and the spin-orbit couplings of the 2p (H_{LS-2p}) and 3d (H_{LS-3d}) electrons [3]:

$$H_{eff} = H_{ELECTRO} + H_{LS-2d} + H_{LS-3d} \quad (2.8)$$

$$H_{ELECTRO} = \langle 2p^5 3d^1 | \frac{e^2}{r_{12}} | 2p^5 3d^1 \rangle \quad (2.9)$$

$$H_{LS-2p} = \langle 2p | \zeta_p \ell_p \cdot s_p | 2p \rangle \quad (2.10)$$

$$H_{LS-3d} = \langle 3d | \zeta_d \ell_d \cdot s_p | 3d \rangle \quad (2.11)$$

The x-ray absorption transition matrix elements to be calculated are:

$$I_{XAS} \propto \langle 3d^0 | p | 2p^5 3d^1 \rangle^2 \quad (2.12)$$

However, to theoretically simulate an x-ray absorption spectrum which lies in close agreement to what is experimentally recorded, one needs to take into account solid state effects. This is done by using the ligand field multiplet model which introduces crystal

³Refer to Appendix B.

field parameters into the calculation. After which, the charge transfer parameters are then included into the calculation.

2.2 Ligand Field Multiplet Theory

The ligand field multiplet (LFM) model approximates a TM as an isolated atom surrounded by a distribution of charges, which mimic the system, molecule, or solid, around the TM [3]. Essentially it is applying a group theoretical treatment to the symmetry operations present in common molecules [12]. The LFM Hamiltonian consists of the atomic Hamiltonian, equation (3), to which a crystal field (CF) is added [3]:

$$H_{LFM} = H_{ATOM} + H_{CF} \quad (2.13)$$

$$H_{CF} = -e\phi(\vec{r}) \quad (2.14)$$

The crystal field consists of the electronic charge e times a potential that describes the surroundings $\phi(\vec{r})$. The potential $\phi(\vec{r})$ is written as a series expansion of spherical harmonics Y_{LM} s [3]:

$$\psi(\vec{r}) = \sum_{L=0}^{\infty} \sum_{M=-1}^L r^L A_{LM} Y_{LM}(\Psi, \psi) \quad (2.15)$$

The crystal field is regarded as a perturbation, thus, the matrix elements of $\psi(\vec{r})$ should be determined with respect to the 3d-orbitals [3].

2.3 Crystal Field Theory

Crystal field theory (CFT) is a model that describes the breaking of degeneracies of electronic orbital states, usually d or f-orbitals, due to a static electric field produced by a surrounding charge distribution. It is developed by considering the energy changes of the five degenerate d-orbitals upon being surrounded by an array of point charges consisting of the ligands. As a ligand approaches the metal ion, the electrons from the ligand will be closer to some of the d-orbitals and farther away from others causing a loss of degeneracy. The electrons in the d-orbitals and those in the ligand repel each other due to repulsion between like charges. Thus, the d-electrons closer to the ligands will have a higher energy than those further away which results in the d-orbitals splitting in energy [13].

Many systems possess a TM ion surrounded by six/eight ligands. The six ligands are positioned on the three Cartesian axes, that is, on the six faces of a cube surrounding the TM. They form the octahedral field. The eight ligands are positioned on the eight corners of the cube and form the cubic field. Both these systems belong to the O_h point

group which is a subgroup of the atomic SO_3 [3]. If one were to rotate a featureless sphere by any angle around any axis running through the sphere's center, it will look exactly the same. This is SO_3 symmetry. O_h stands for full octahedral symmetry and is the full symmetry group of the cube and octahedron.

To calculate an x-ray absorption spectrum in a cubic crystal field, the atomic transition matrix elements must be branched from an SO_3 (spherical) symmetry to an O_h (cubic) symmetry [3]. The CTM4XAS 5.2 program implements this by running a program called RAC2 which applies the necessary branching rules determined from group theory [14]. One can lower the symmetry even further from O_h symmetry to D_{4h} (tetragonal) symmetry by applying another set of branching rules, again determined from group theory. D_{4h} is a subgroup of O_h and belongs to the prismatic groups. In group theory terms, this can be imagined as a coloured cube where two of the opposite faces have the same color whilst all other faces have one different color. For TiO_2 , this translates as a stretching along one of its lattice vectors, resulting in a stretched cube shape, as can be seen in Figure 2.1.

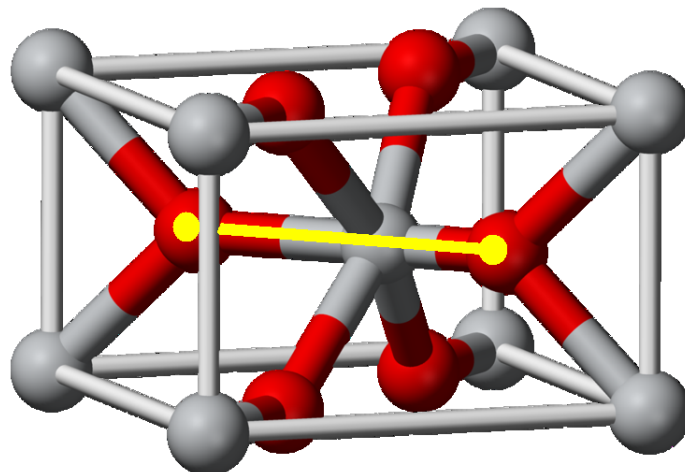


Figure 2.1: Rutile titanium oxide unit cell, where the stretched lattice vector is indicated by the yellow line.

The radial parameters related to these branches are indicated as X_{40} , X_{400} , X_{420} , and X_{220} and can be related to other definitions such as $10 Dq$, Ds , and Dt by comparing their effects on the set of 3d functions. The most straightforward way to specify the strength of the crystal field parameters is to calculate the energy separations of the 3d functions. In O_h symmetry, there is only one crystal field parameter X_{40} . This parameter is normalized in a manner that creates unitary transformations in the calculations. Table 2.1 shows the relation between the linear combination of X parameters to the linear combination of the Dq , Ds , and Dt parameters, and the specific 3d orbitals they represent.

Table 2.1: Energy of the 3d Orbitals Is Expressed In X_{400} , X_{420} , and X_{220} in the First Column and in Dq, Ds, and Dt in the Second Coloumn [3].

Energy Expressed in X-Terms	In D-Terms	Orbitals
$30^{-1/2} \cdot X_{400} - 42^{-1/2} \cdot X_{420} - 2 \cdot 70^{-1/2} \cdot X_{220}$	$6Dq + 2Ds - 1Dt$	$x^2 - y^2$
$30^{-1/2} \cdot X_{400} + 42^{-1/2} \cdot X_{420} + 2 \cdot 70^{-1/2} \cdot X_{220}$	$6Dq - 2Ds - 6Dt$	z^2
$-2/3 \cdot 30^{-1/2} \cdot X_{400} + 4/3 \cdot 42^{-1/2} \cdot X_{420} - 2 \cdot 70^{-1/2} \cdot X_{220}$	$-4Dq + 2Ds - 1Dt$	xy
$-2/3 \cdot 30^{-1/2} \cdot X_{400} - 2/3 \cdot 42^{-1/2} \cdot X_{420} + 70^{-1/2} \cdot X_{220}$	$-4Dq - 1Ds + 4Dt$	xz, yz

From this table, one can relate both notations and write X_{400} , X_{420} , and X_{220} as a function of Dq, Ds, and Dt:

- $X_{400} = 6 \cdot 30^{1/2} \times Dq - \frac{7}{2} \times 30^{1/2} \times Dt$
- $X_{420} = -\frac{5}{2} \times 42^{1/2} \times Dt$
- $X_{220} = -70^{1/2} \times Ds$

In octahedral symmetry, the crystal field parameters split a 3d configuration into an e_g and a t_{2g} configuration. t_{2g} consists of the d_{xy} , d_{xz} , and d_{yz} orbitals which will be lower in energy than the e_g configuration, consisting of the higher energy d_{z^2} and $d_{x^2-y^2}$ orbitals. The reason the t_{2d} group is lower in energy is because it is farther from the ligands than the e_g group and therefore experiences less repulsion [13]. In D_{4h} symmetry, the t_{2g} and e_g symmetry states split further into e_g and b_{2g} , respectively, and a_{1g} and b_{1g} . Depending on the nature of the tetragonal distortion, either the e_g or the b_{2g} state have the lowest energy [3].

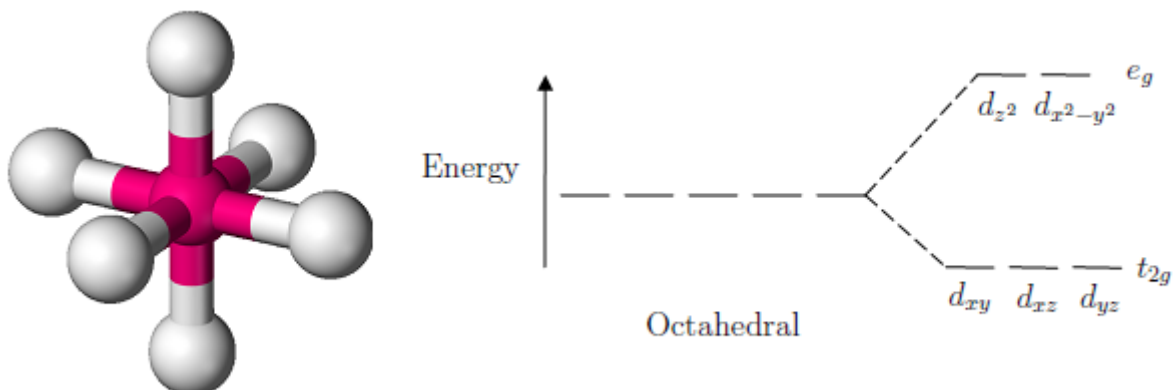


Figure 2.2: The geometric shape of octahedral symmetry is represented on the left, whilst it's crystal field splitting diagram is to the left

2.4 Charge Transfer Multiplet Theory

Charge transfer effects are the effects of charge fluctuations in the initial and final states. In atomic multiplet and LFM theories, a single configuration is used to describe the ground state and final state. In the charge-transfer model, however, two or more configurations are used. It does this by adding the configuration $3d^{n+1}\underline{L}$ to the $3d^n$ ground state. In the case of a TM oxide, in a $3d^{n+1}\underline{L}$ configuration an electron has been moved from the oxygen 2p valence band to the metal 3d band. One can continue with this procedure and add a $3d^{n+2}\underline{L}^2$ configurations, and so on. In many cases, two configurations are enough to explain the spectral shapes of XAS. Unless one is dealing with a high valence state where it can be important to include more configurations [3].

The charge-transfer effect adds a second dipole transition, a second initial state, and a second final state. The two initial states and two final states are coupled by hybridization (i.e. the charge-transfer effect between the ligand p and the TM 3d states). The mixing Hamiltonian is given by

$$H_{MIX} = \sum_v V(\Gamma)(a_{dv}^+ a_v + a_v^+ a_{dv}) \quad (2.16)$$

The XAS spectrum is calculated by solving the equations (2.17) and (2.18) below.

$$M_{I1,I2} = \langle 3d^n | H_{MIX} | 3d^{n+1}\underline{L} \rangle \quad (2.17)$$

$$M_{F1,F2} = \langle 2p^5 3d^{n+1} | H_{MIX} | 2p^5 3d^{n+2}\underline{L} \rangle \quad (2.18)$$

In the CTM4XAS 5.2 program, the charge transfer effects can be altered using a seven different parameters. The first is the charge transfer energy, Δ , which gives the energy difference between the (centers of the) $3d^n$ and the $3d^{n+1}\underline{L}$ configurations. The effective value of Δ is affected by the multiplet and crystal field effects on each configuration. The second is U_{dd} which is the value of the on-site dd Coulomb repulsion energy. The third is U_{pd} which is the core hole potential [3]. In the case of XAS spectra, only the difference between U_{pd} and U_{dd} is important. The remaining parameters, a_1 , b_1 , e , and b_2 (the four symmetries in tetragonal symmetry), are known as the hopping parameters. a_1 (z^2) and b_1 ($x^2 - y^2$) are part of the e_g -orbitals. e (xz, yz) and b_2 (xy) are part of the t_{2g} -orbitals. In O_h symmetry their values are $a_1 = b_1$ and $e = b_2$ [14].

2.5 Resonant Inelastic X-Ray Scattering

By considering the entire process of RIXS as a set of atomic state transitions from ground state $|g\rangle$ to an intermediate state $|i\rangle$ to a final state $|f\rangle$ of energies E_g , E_i , and E_f respectively, one can define the Kramers-Heisenberg equation for the scattering cross section, σ , as

$$\sigma(\Omega, \omega) \propto \sum_j \left[\sum_i \frac{\langle j|T|i\rangle \langle i|T|g\rangle}{E_g + \Omega - E_i - i\Gamma_i} \right]^2 \times \delta(E_g + \Omega - E_j - \omega) \quad (2.19)$$

where T represents the radiative transition and Γ_i is the broadening due to the intermediate state core-hole lifetime [1]. The resonant behaviour arises at the absorption threshold as the denominator terms E_g , Ω , and E_i , cancel leaving only the core-hole broadening [1].

2.6 Spectroscopic Simulation Software

Throughout this project one used the programs CTM4XAS 5.2 and CTM4RIXS to carry out all theoretical simulations. The source codes for the CTM4XAS 5.2 calculations are the TT-MULTIPLY charge transfer multiplet programs, as have been originally developed by Theo Thole and modified by Haruhiko Ogasawara. The Charge Transfer multiplet program is a semi-empirical program that includes explicitly the important interactions for the calculation of L -edge spectra. Interactions such as the core and valence spin-orbit coupling, the core-valence overlap (multiplet effects), and the effects of strong correlations within the charge transfer model [11].

CTM4XAS 5.2 calls and combines different programs to compute simulations. The first program to be called is RCN2, which is used to compute the atomic parameters. RCN2 can calculate any element and any transition in the periodic table. The only information needed is the atomic number and the initial and final state configurations. The Slater integrals (F^2 , G^1 , and G^3) are scaled down to 80% of their ab initio values [8]. If one would like the atomic multiplet spectrum to be calculated for the input of RCN2, another program called RCG2 is executed. The CTM4XAS 5.2 program then runs RAC2, which calculates the crystal field multiplets using the output obtained from RCN2. The reduced matrix elements of all necessary operators in the spherical group are calculated with the use of Cowan's atomic multiplet program. To obtain the reduced matrix elements in any point group, Butler's program is used for the calculation of all necessary factors (3J symbols) [8]. The results of these two programs are written to matrix files. These matrices are then used by an additional program called BAN2 to generate the charge transfer multiplet spectrum [14].

Chapter 3

Computational Method

To simulate XAS spectra, the program ‘CTM4XAS 5.2’ was utilised. For RIXS simulation, the program ‘CTM4RIXS’ was employed [11].

3.1 Method for Simulating XAS

CTM4XAS 5.2 was started by running the CTM4XAS52.exe file. This opened the parameter window, as can be seen in Figure 3.1.

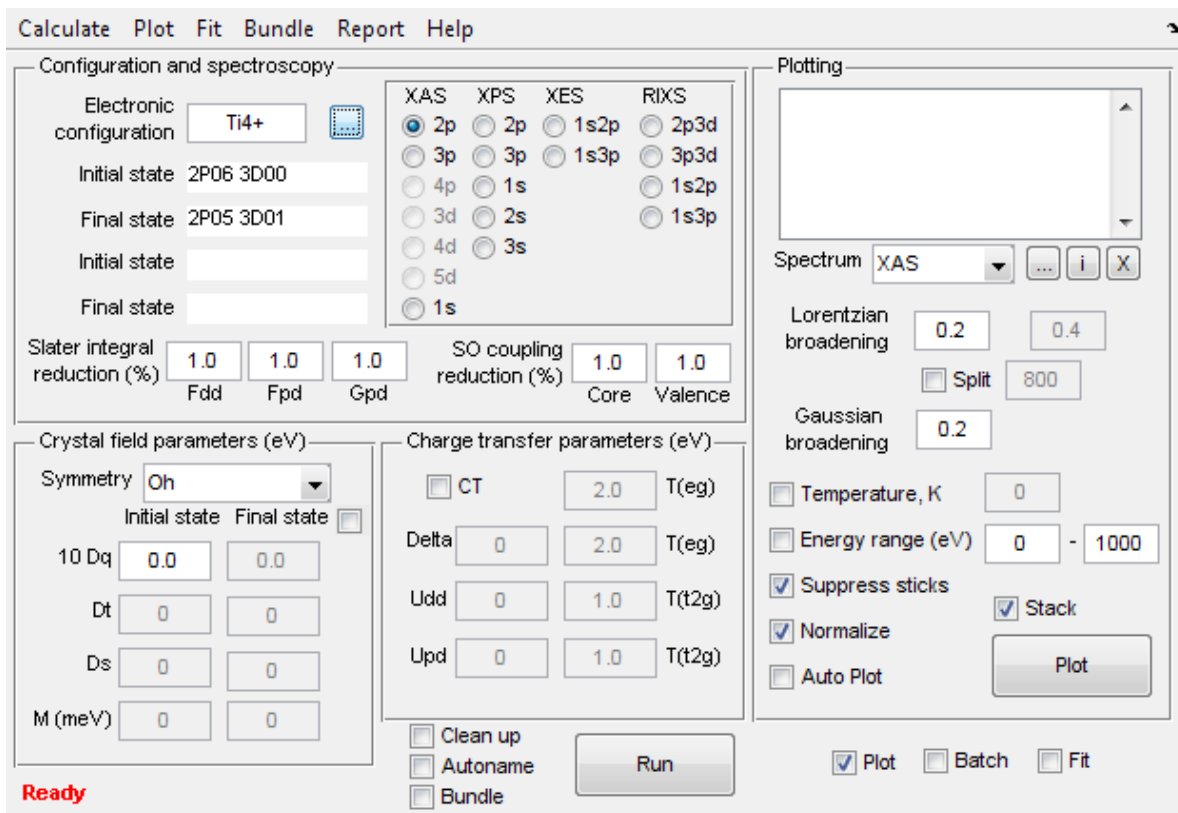


Figure 3.1: CTM4XAS52 Parameter Window

1. The first step was to define the configuration to be calculated. This was done by clicking on the blue highlighted box located in the ‘Configuration and spectroscopy’ partition, beside ‘Electronic configuration’ in Figure 3.1. One then selected the desired element and valence. This automatically filled the ‘Initial state’ and ‘Final state’ boxes.
2. Next, the type of spectroscopy to be simulated was selected from the list of available options. These were contained in the bordered area beside the blue highlighted button in Figure 3.1. The orbitals to be probed were also selected here. Every XAS simulation in this project was carried out with ‘2p’ selected.
3. The ‘Slater integral reduction (%)’ parameters F_{dd} , F_{pd} , and G_{pd} , were all left at their default values of ‘1.0’ for the duration of the project.
4. The ‘SO coupling reduction (%)’ parameters ‘Core’ and ‘Valence’, were also left at their default values of ‘1.0’ for the duration of the project.
5. The ‘Crystal field parameters (eV)’ partition contained options to define the type of symmetry and crystal field one wished to be applied. The default setting was O_h symmetry which only allowed the crystal field parameter ‘10 Dq’ to be defined. When necessary, however, it was changed to other symmetries via the arrow button beside it, which produced a drop down menu containing the other options such as D_{4h} symmetry, which was also used for calculations in this project.
6. When the symmetry was changed to D_{4h} , the crystal field parameter ‘Dt’ and ‘Ds’, in addition to ‘10 dq’, were made available. The desired values were then filled in and the ‘Final state’ state box selected.
7. For charge-transfer calculation, one selected the box ‘CT’ to activate the ‘Charge transfer parameters (eV)’ partition. The parameter ‘Delta’, ‘ U_{dd} ’, and ‘ U_{pd} ’ were then changed to the desired values. The remaining parameters within this partition, remained at their default values: $T(\text{eg})=2.0$, $T(\text{eg})=2.0$, $T(\text{t2g})=1.0$, and $T(\text{t2g})=1.0$, for all simulations.
8. Within, the ‘Plotting’ partition’, the ‘Split’ button was selected and changed to ‘461’. The ‘Gaussian broadening’ was changed to ‘0.1’. The ‘Suppress sticks’ button was de-selected. The remaining operations were left at their default values.
9. Finally, the button ‘Run’, located at the bottom of the screen, was selected, which prompted one to name and save the calculation. After which, the software began a series of calculations using the RCN2, RCG2, RAC2, BAN2, and PLO2 programs described in chapter 2.

Although values for the Lorentzian broadening were defined in point 8. These were improved upon manually, imposing a different broadening for each peak. This allowed for a better fit to experiment. The details of the method used to do this can be found in Appendix B, Section 5.3.2.1.

Simulations were plotted using Origin 8 where the output file from the PLO2.exe, [filename].dat was imported as a single ASCII. Theoretical spectra were layered onto already imported experimental spectra such that their energy values, along the x-axis, aligned.

3.2 Method for Simulating RIXS

The first part of the RIXS calculation was carried out in the CTM4XAS 5.2 program exactly as recounted in steps 1-9 for XAS calculations, except, instead of selecting the 2p XAS button, one chose the 2p-3d RIXS button. Once the calculation was complete, CTM4RIXS was started by running the CTM4RIX.exe file. This opened the parameter window. A picture of which can be found in Appendix B, Section 5.2.2.

1. First, one loaded the .ora files computed by the CTM4XAS 5.2 calculation for absorption (in the first box) and for emission (in the second box). ‘Auto output’ and ‘Print energies and matrices’ were both selected. The ‘Create’ button was then clicked and a pop out box appeared to which [1 5] was entered. One then clicked OK and the program created the matrices.
2. The output automatically appeared in the next parameter box ‘AE matrix’, thus, one clicked ‘Combine’. Another pop up box appeared where one chose the ground level to be 1. One then clicked OK and the program combined the created matrices from the first step.
3. Again, the output automatically appeared in the CB matrix box. The RIXS button was clicked and the results were automatically plotted within the program itself. They were then extracted, and graphed with in Origin.

Chapter 4

Results and Discussion

The overall aim of this project was to simulate the metal L -edge 2p-3d resonant inelastic x-ray scattering spectrum of Ti^{3+} , for comparison to a previously obtained experimental RIXS spectrum. Moreover, one also investigated the relationship between the parameters used for Ti^{4+} and Ti^{3+} . This was done by examining whether the values used for parameters in Ti^{4+} calculations, could accurately simulate Ti^{3+} spectra. Simulations were also compared to experimental data which acted as a reference to how simulated spectra should appear, as well as displaying how characteristics within spectra were altered or manipulated by different theoretical parameters.

The first section of results, deals with one's simulation of Ti^{4+} 2p-3d XAS of TiO_2 in octahedral and tetragonal symmetry. The second section, depicts calculations computed for Ti^{3+} 2p-3d XAS, also in octahedral and tetragonal symmetry. The final section presents one's calculation of Ti^{3+} 2p-3d RIXS spectrum. For the Ti^{4+} calculations, I used an experimental XAS rutile TiO_2 Ti L -edge spectrum provided by Declan Cockburn [2] for comparison. For the Ti^{3+} calculations, I used an experimental XAS sputtered rutile TiO_2 Ti L -edge spectrum provided by Stephan Callaghan [15] for comparison. The Ti^{3+} RIXS calculation is compared against experimental RIXS spectra of LAO3 SL excited across the Ti^{3+} 2p_{3/2}-3d e_g threshold from a paper by Ke-Jin Zhou [16].

4.1 Simulated Ti^{4+} 2p XAS

I began by investigating how to simulate Ti^{4+} 2p XAS of TiO_2 . This was done in a step by step process, where new parameters were introduced one by one to determine the effects of each on spectra. Ti^{4+} was investigated first in octahedral symmetry (O_h) and then in tetragonal symmetry (D_{4h}). The parameters that were examined were the crystal field relations and charge-transfer effects.

4.1.1 Octahedral Symmetry

The first task was to find the best value of $10 Dq$ for a Ti^{4+} multiplet calculation in O_h symmetry. In octahedral symmetry, $10 Dq$ is defined as the energy difference between the t_{eg} states and the e_g states, neglecting all atomic parameters [11]. Thus, the best fit $10 Dq$ was found by exploring how changing the value of $10 Dq$ affected the overall shape of the spectrum. Examples of simulated spectra with varying values of $10 Dq$ can be found in Appendix C, Section 5.3.1. Figure 4.1 below illustrates the simulated spectrum, in red, of a Ti^{4+} 2p XAS calculation where $10 Dq=1.8$ eV. This is compared against an experimental XAS spectrum, in black, of a rutile TiO_2 Ti L -edge.

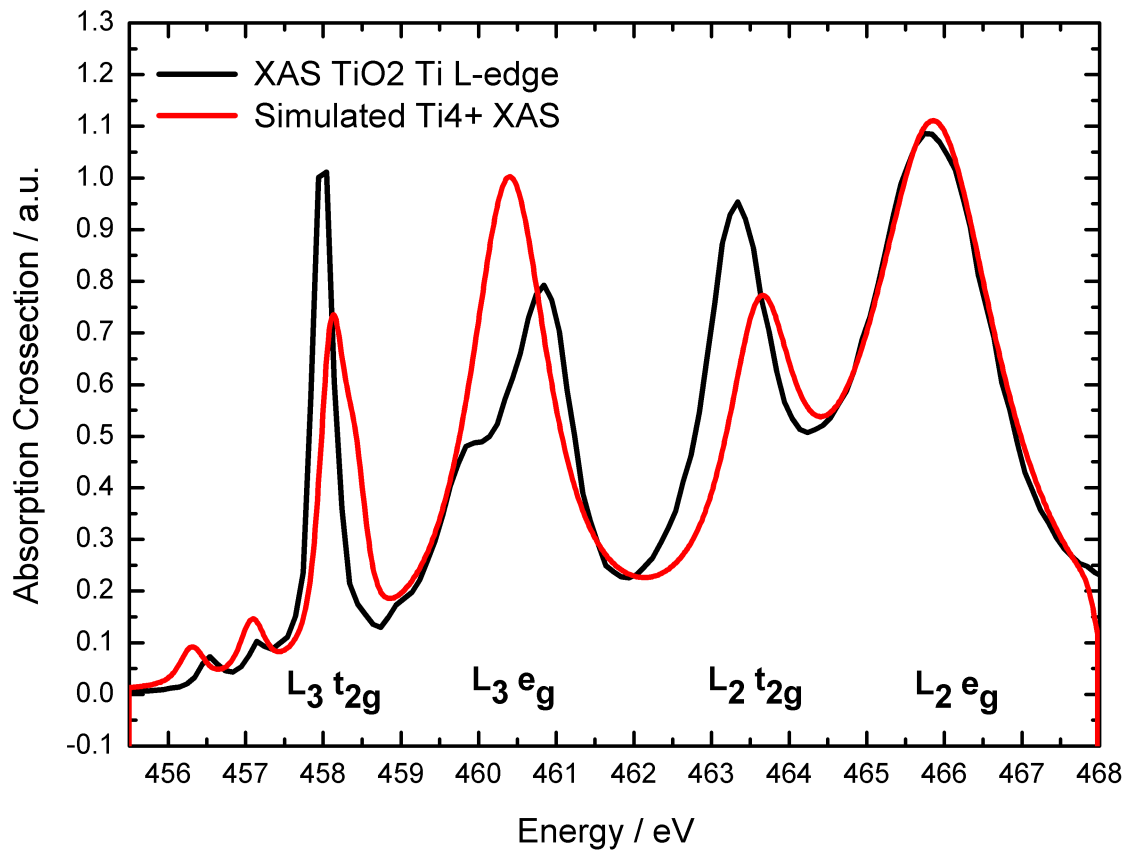


Figure 4.1: The simulated XAS spectrum (in red) of a 2p Ti^{4+} calculation in O_h symmetry with $10 Dq=1.8$ eV, compared against an experimental XAS spectrum (in black) of rutile TiO_2 Ti L -edge. The Lorentzian broadening values used for each peak in the simulated spectrum were 0.1 eV, 0.6 eV, 0.5 eV, and 1.0 eV going from left to right respectively.

As one can see, in octahedral symmetry, the value of $10 Dq=1.8$ eV compares nicely against the overall shape of the experimental data. The crystal field parameter has split the $2p_{3/2}$ (L_3) and $2p_{1/2}$ (L_2) into two more peaks known as t_{eg} and e_g . Thus, four peaks in total are present, in order of increasing energy known as the $L_3 t_{2g}$, $L_3 e_g$, $L_2 t_{2g}$ and $L_2 e_g$ features.

The crystal field parameter, $10 Dq$, clearly has a large influence on the simulated XAS Ti^{4+} spectrum. The other crystal field parameters Ds and Dt are not included as in O_h symmetry as $Ds=Dt=0$. Hence, the next step was to record a simulated spectrum including charge-transfer effects. Figure 4.2 shows the simulated spectrum of a Ti^{4+} 2p-3d XAS in O_h symmetry including $10 Dq$ and charge-transfer effects Δ , U_{dd} , and U_{pd} (obtained from Matsubara et al (2000) paper [17]), compared against an experimental XAS Ti L -edge.

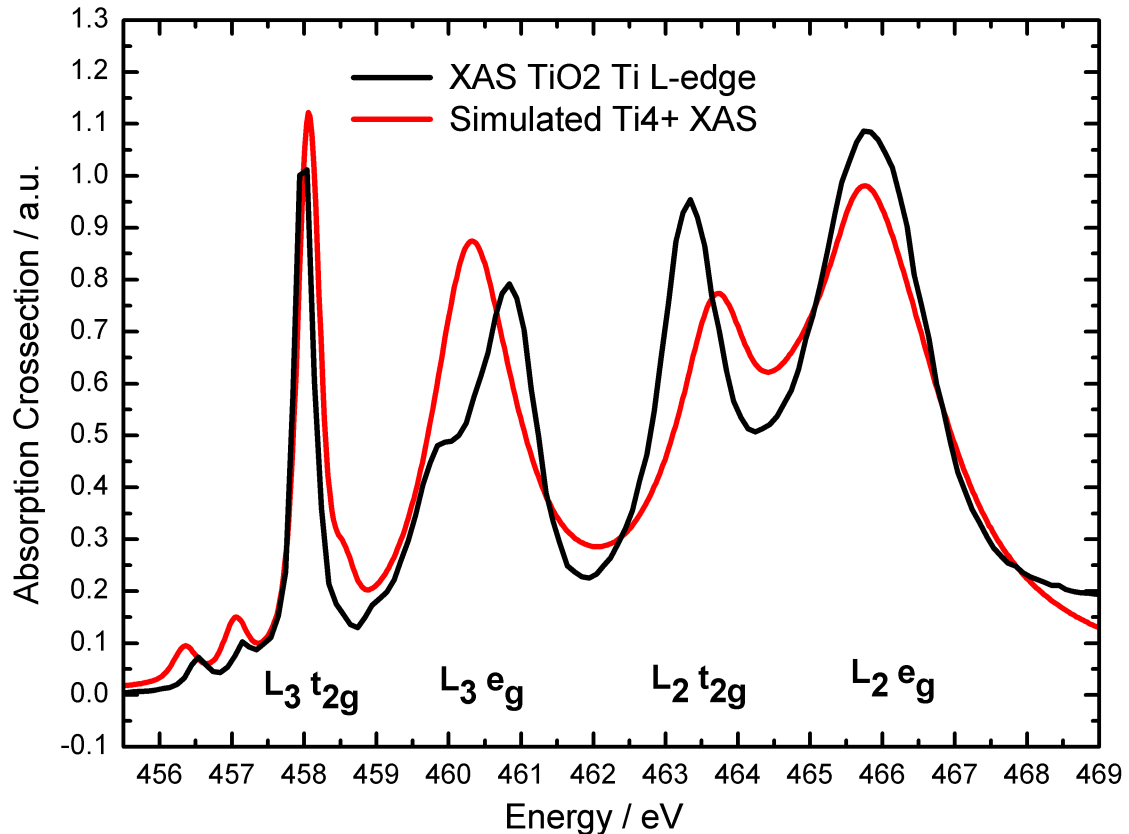


Figure 4.2: The simulated XAS spectrum (in red) of a 2p Ti^{4+} calculation in O_h symmetry with $10 Dq=1.7$ eV, $\Delta=2.98$ eV, $U_{dd}=4.0$ eV, and $U_{pd}=6.0$ eV, compared against an experimental XAS spectrum (in black) of rutile TiO_2 Ti L -edge. The Lorentzian broadening values used for each peak in the simulated spectrum were 0.1 eV, 0.6 eV, 0.5 eV, and 1.0 eV going from left to right respectively.

From Figure 4. the $L_3 t_{2g}$ peak increases in intensity whereas the L_3 and $L_2 e_g$ peaks, each slightly decrease in intensity. According to DeGroot [3], for systems with a positive value of Δ , the main effects on the XAS spectral shape are, the formation of small satellites and contraction of the multiplet structures. The latter is visible with regards to L_3 and $L_2 e_g$ peaks, however, no satellites seem to be present. In any case, the formation of small satellites or even the absence of visible satellite structures is a special feature of XAS. This is because the local charge of the final state is equal to the charge of the initial state. Implying that there is little screening and thus, few charge-transfer satellites [3].

4.1.2 Tetragonal Symmetry

The O_h calculation in section 4.2 is a good start, however, more parameters need to be incorporated if one is to achieve a simulation as close as possible to experimental spectra. As was explained in section 2.2, the TiO_2 rutile unit cell is not in fact a perfect octahedral. Instead, it is distorted, where one of its lattice vectors is stretched, as can be seen in Figure 2.1. This is due to the arrangement of oxygen ligands about the Ti^{4+} ion. Thus, due to these longer Ti-O bonds along only one of the axis, the point group symmetry of the cation is reduced from O_h to D_{4h} . Figure 4.3 displays the results of a Ti^{4+} multiplet calculation in D_{4h} symmetry.

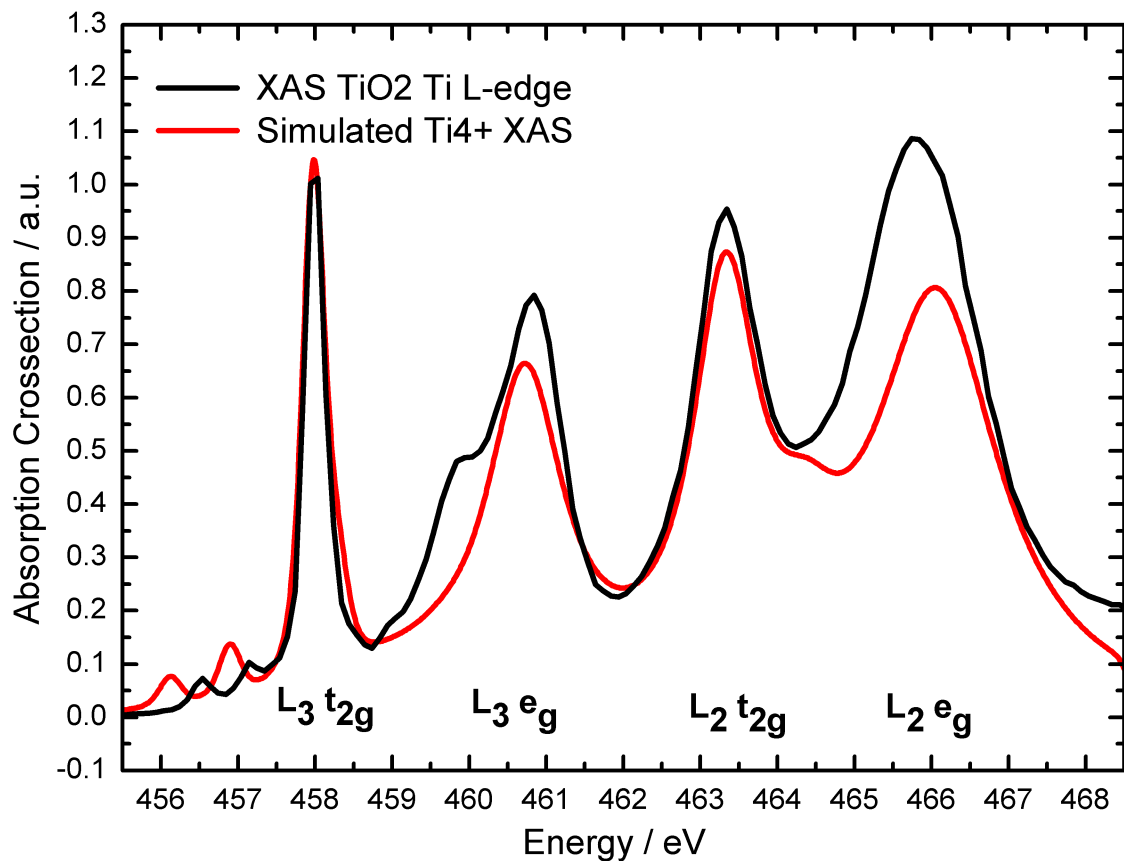


Figure 4.3: The simulated XAS spectrum (in red) of a 2p Ti^{4+} calculation in D_{4h} symmetry with $10 Dq=2.8$ eV, $Dt=0.0771$ eV, and $Ds=0.1286$ eV. These were derived from the experimental spectrum itself using a method outlined in Appendix C, Section 5.3.2. Compared against an experimental XAS spectrum (in black) of rutile TiO_2 Ti L -edge. The Lorentzian broadening values used for each peak in the simulated spectrum were 0.1 eV, 0.6 eV, 0.5 eV, and 1.0 eV going from left to right respectively.

The simulated XAS in D_{4h} symmetry is definitely a better comparison of the experimental XAS than the previous simulations in O_h symmetry. However, the splitting of the e_g state appears to be completely absent from the calculation, despite deducting values for $10 Dq$, Ds , and Dt from the experimental data. This I feel is down to the broadening

used, perhaps the Lorentzian broadening of 0.6 eV, applied to the $L_3 e_g$ feature was too high. If I were to do this calculation again I would reduce this to 0.5 eV.

Next, was to explore the charge-transfer effects in D_{4h} symmetry on Ti^{4+} XAS spectra. Figure 4.4 shows the Ti^{4+} 2p-3d XAS calculation including crystal field and charge transfer effects where were obtained from Matsubara et al (2000) paper [17], compared against an experimental XAS Ti L -edge.

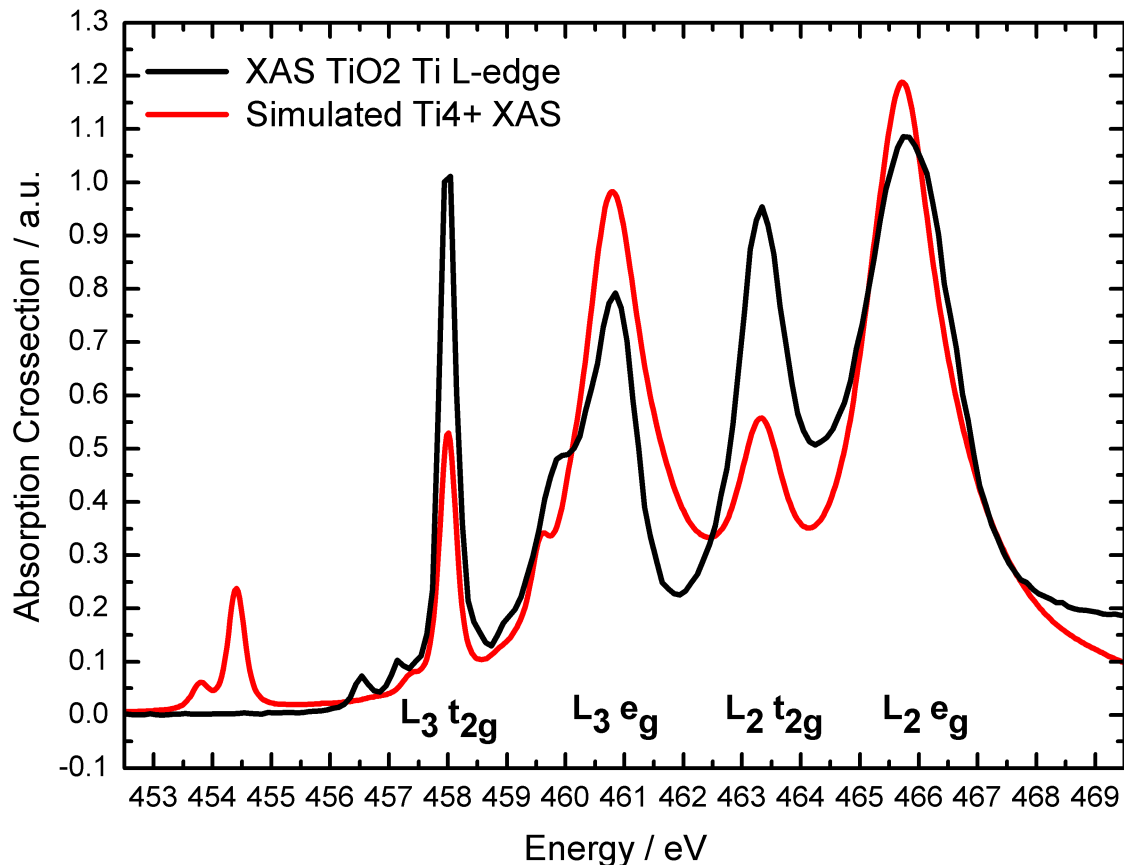


Figure 4.4: The simulated XAS spectrum (in red) of a 2p Ti^{4+} calculation in D_{4h} symmetry with $10 Dq=1.7$ eV, $Ds=0.9$ eV, $Dt=0.8$ eV $\Delta=2.98$ eV, $U_{dd}=4.0$ eV, and $U_{pd}=6.0$ eV, compared against an experimental XAS spectrum (in black) of rutile TiO_2 Ti L -edge. The Lorentzian broadening values used for each peak in the simulated spectrum were 0.1 eV, 0.6 eV, 0.5 eV, and 1.0 eV going from left to right respectively.

Unlike the previous charge-transfer calculation in O_h symmetry, the t_{2g} peaks appear to have increased in absorption intensity, whereas the e_g peaks have contracted. There is also the appearance of small charge-transfer satellites, which were absent from the previous O_h calculation. Another feature which appears, is a small initial peak in the $L_3 e_g$ edge relating to the dz^2 state which becomes degenerate in D_{4h} symmetry. Although, features relating to the parameters applied are present, the overall shape of the spectrum is not a good comparison to experimental data. This could be because all the values for the crystal field and charge-transfer were from Matsubara et al (2000) paper [17].

Since I had already worked out the crystal field parameters in relation to the actual experimental spectrum I was comparing my calculations against, I decided to repeat the calculation using those crystal field values and broadenings, but kept the charge-transfer values the same as the Matsubara et al (2000) paper [17]. Figure 4.5 shows the results.

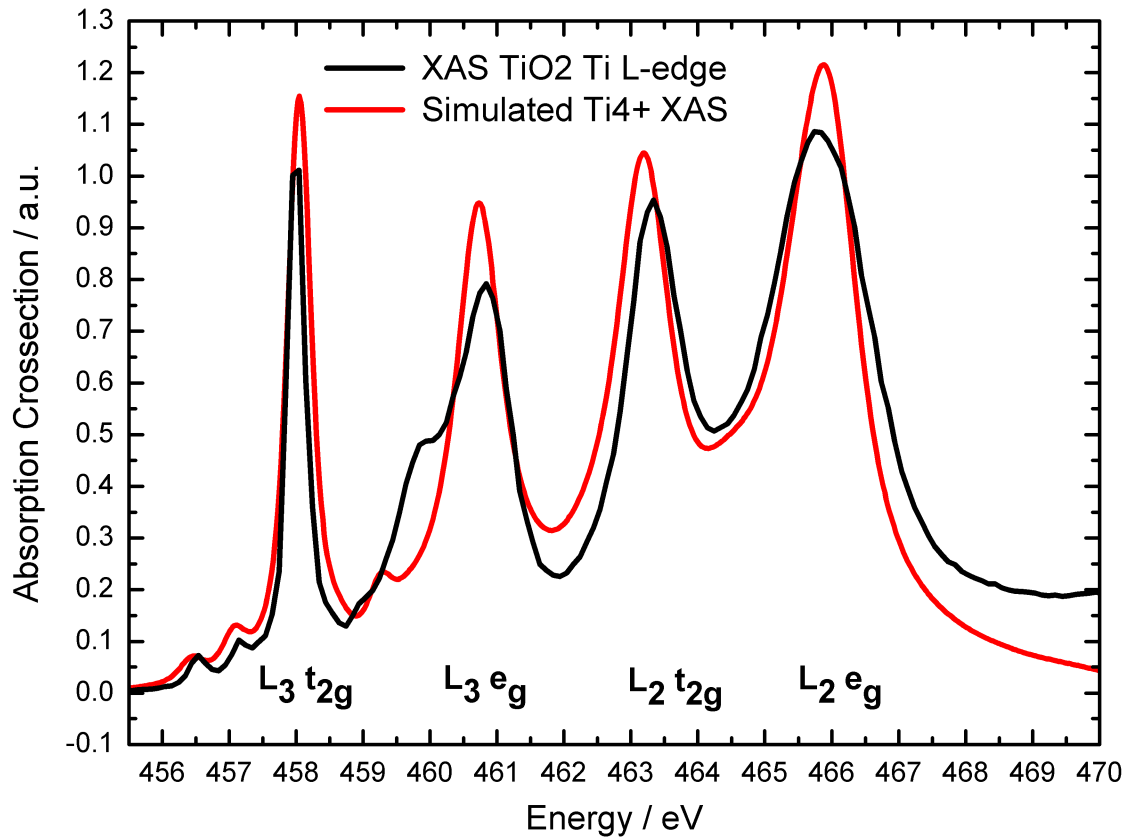


Figure 4.5: The simulated XAS spectrum (in red) of a 2p Ti^{4+} calculation in O_h symmetry with $10 Dq=2.8$ eV, $Ds=0.1286$ eV, $Dt=0.00771$ eV $\Delta=2.98$ eV, $U_{dd}=4.0$ eV, and $U_{pd}=6.0$ eV, compared against an experimental XAS spectrum (in black) of rutile TiO_2 Ti L -edge. The Lorentzian broadening values used for each peak in the simulated spectrum were 0.175 eV, 0.4 eV, 0.45 eV, and 0.5 eV going from left to right respectively.

This concurs much better with the experimental XAS, and, although small, the dz^2 peak is still present. Figure 4.5 shows just how important it is to choose the right broadenings.

4.2 Simulated Ti^{3+} 2p-3d XAS

Ti^{3+} 2p-3d XAS multiplet calculations were carried out for TiO_2 to understand and to see if one could simulate surface effects by using the same parameters used for Ti^{4+} applied to a Ti^{3+} configuration. Examples of such surface effects include a missing oxygen and reduced coordination at the surface, or surface reduction to Ti_2O_3 , or an oxygen vacancy resulting in the subsequent creation of Ti^{3+} ions surrounding the oxygen vacancy.

4.2.1 Octahedral Symmetry

The first calculation mimics that for Ti^{4+} in O_h symmetry except applied to Ti^{3+} . Figure 4.6 displays the resulting spectrum in blue.

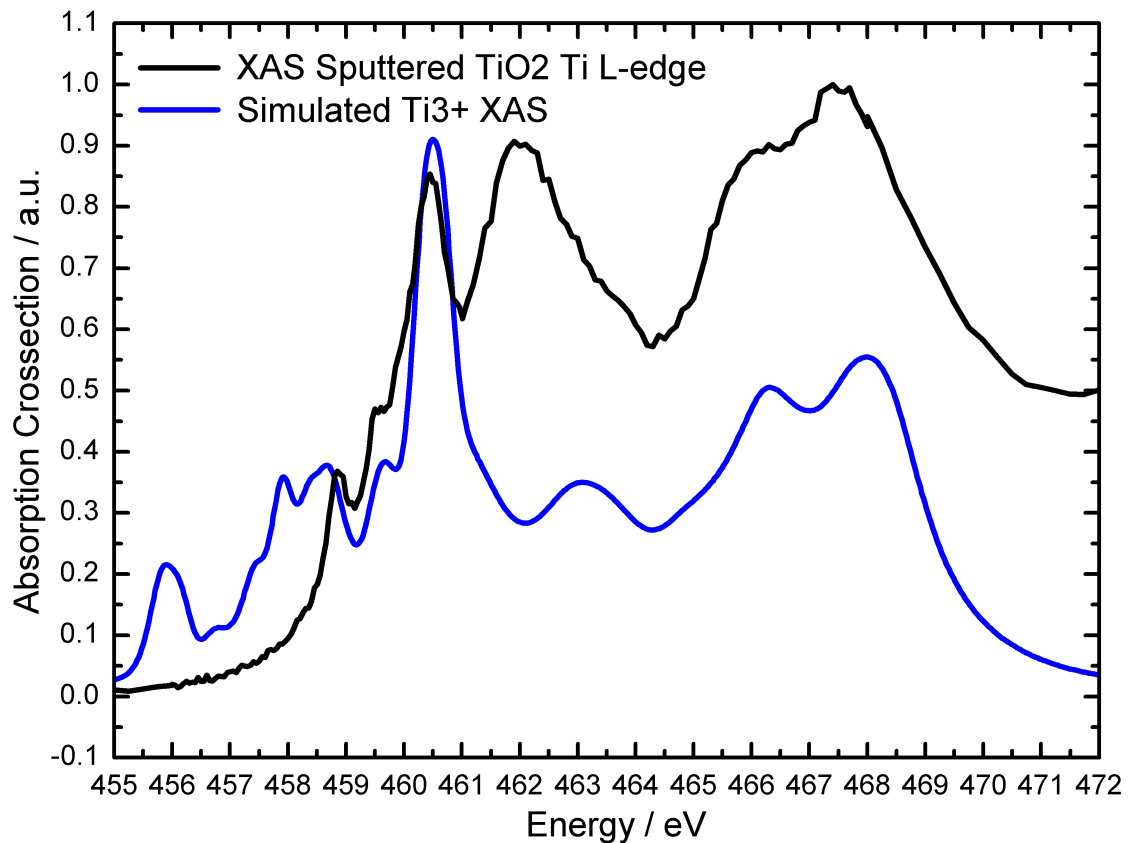


Figure 4.6: The simulated XAS spectrum (in red) of a 2p Ti^{3+} calculation in O_h symmetry with $10 Dq=1.8$ eV, compared against an experimental XAS spectrum (in black) of sputtered rutile TiO_2 Ti L -edge. The Lorentzian broadening values used for each peak in the simulated spectrum were 0.1 eV, 0.6 eV, 0.5 eV, and 1.0 eV going from left to right respectively.

Although, the $L_3 t_{eg}$ peak appears to correspond to the that of the sputtered experimental spectrum, apart from that there appears to be little agreement between the two.

This maybe to be expected since the calculation is in O_h symmetry. If surface effects such as oxygen vacancies etc. were present, the point-group symmetry would greatly reduced.

Figure 4.7 depicts the simulated spectrum of the same calculation as that for Ti^{4+} with charge-transfer effects in O_h symmetry except applied to a Ti^{3+} configuration instead.

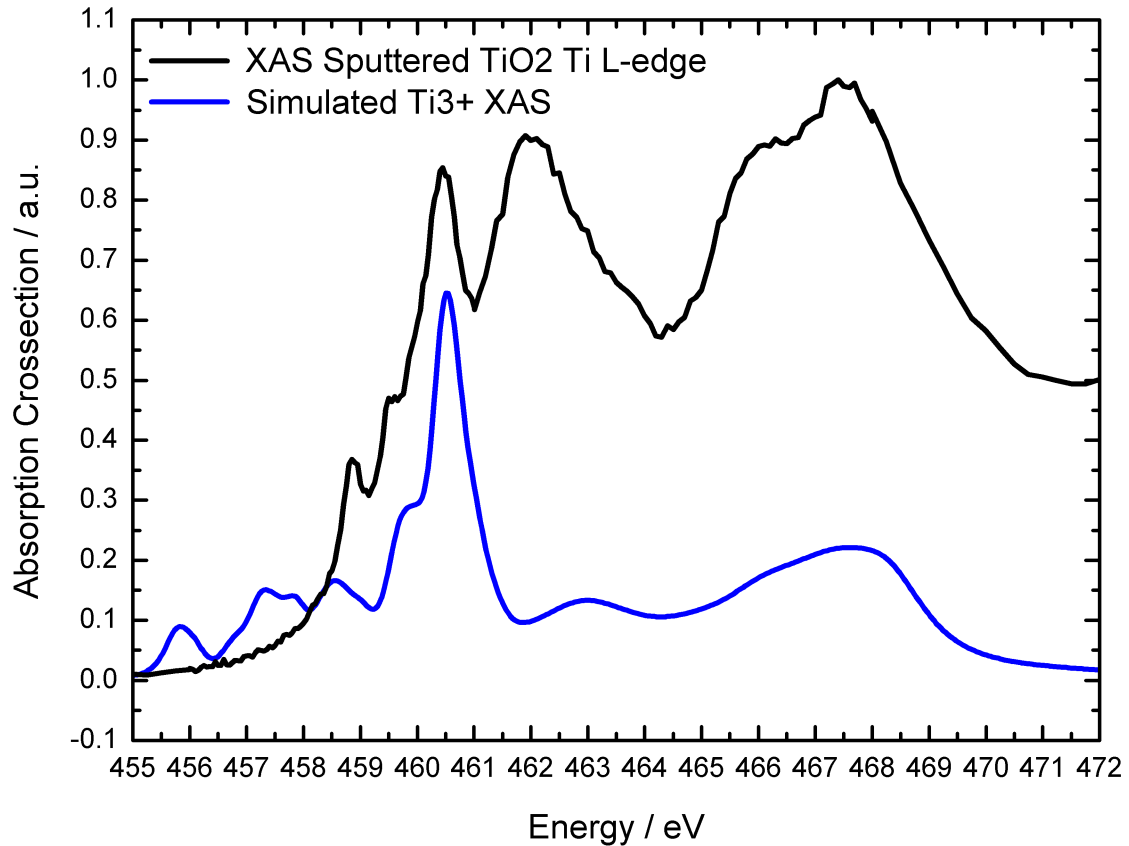


Figure 4.7: The simulated XAS spectrum (in red) of a 2p Ti^{3+} calculation in O_h symmetry with $10 Dq=1.7$ eV, $\Delta=2.98$ eV, $U_{dd}=4.0$ eV, and $U_{pd}=6.0$ eV, compared against an experimental XAS spectrum (in black) of sputtered rutile TiO_2 Ti L -edge. The Lorentzian broadening values used for each peak in the simulated spectrum were 0.1 eV, 0.6 eV, 0.5 eV, and 1.0 eV going from left to right respectively.

At first glance, this calculation appears to disagree even more so with the sputtered experimental XAS than the previous calculation without charge-transfer. However, the $L_3 e_g$ and L_2 feature seem far to muted, and I expect the discrepancy to be due to one's choice of broadenings, the same used for Ti^{4+} . Thus, one can concluded that so far, Ti^{4+} broadening cannot be applied to Ti^{3+} 2p-3d XAS multiplet calculations. To accurately describe broadenings for Ti^{3+} one needs to adjust them according to the experimental data.

4.2.2 Tetragonal Symmetry

Figure 4.8 is the Ti^{3+} 2p-3d TiO_2 XAS multiplet calculation in d_{4h} symmetry, using the same values defined for the equivalent Ti^{4+} calculation, compared against the experimental XAS of a sputtered rutile TiO_2 sample.

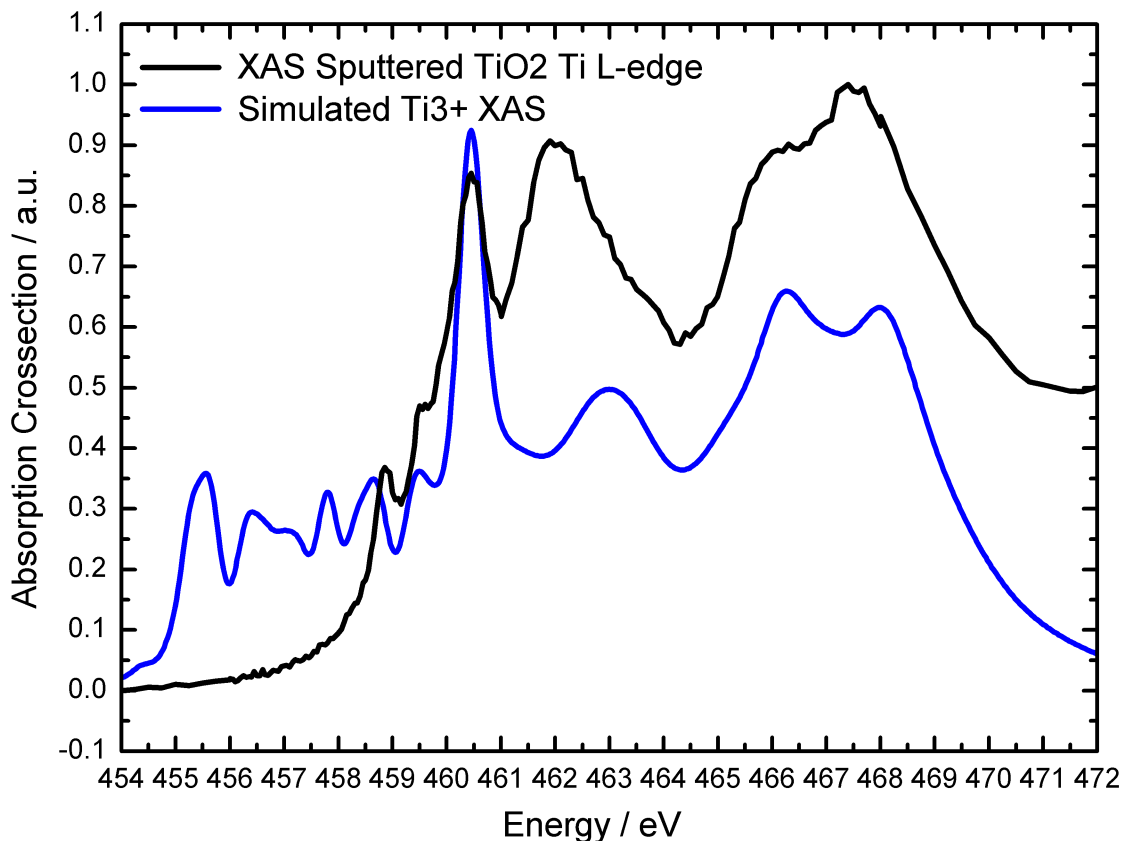


Figure 4.8: The simulated XAS spectrum (in red) of a 2p Ti^{3+} calculation in D_{4h} symmetry with $10 Dq=2.8$ eV, $Dt=0.0771$ eV, and $Ds=0.1286$ eV. Compared against an experimental XAS spectrum (in black) of sputtered rutile TiO_2 Ti L -edge. The Lorentzian broadening values used for each peak in the simulated spectrum were 0.1 eV, 0.6 eV, 0.5 eV, and 1.0 eV going from left to right respectively. The $10 Dq$ parameters in this calculation were worked out from the experimental spectrum, the method of which is outlined in Appendix C, Section 5.3.2.

The simulated spectrum is quite reminiscent of that calculated in O_h Ti^{3+} without charge-transfer effects and perhaps may fit better to the experimental data if the Lorentzian broadenings were adjusted. If I were to repeat this calculation, in particular, the broadenings applied to the L_2 features would be lowered.

Finally, the Ti^{4+} calculation in D_{4h} symmetry with charge-transfer effects was repeated for the Ti^{3+} configuration. Figure 4.9 shows the Ti^{3+} 2p-3d XAS calculation including crystal field and charge transfer effects where were obtained from Matsubara et al (2000) paper [17], compared against an experimental XAS sputtered rutile Ti L -edge.

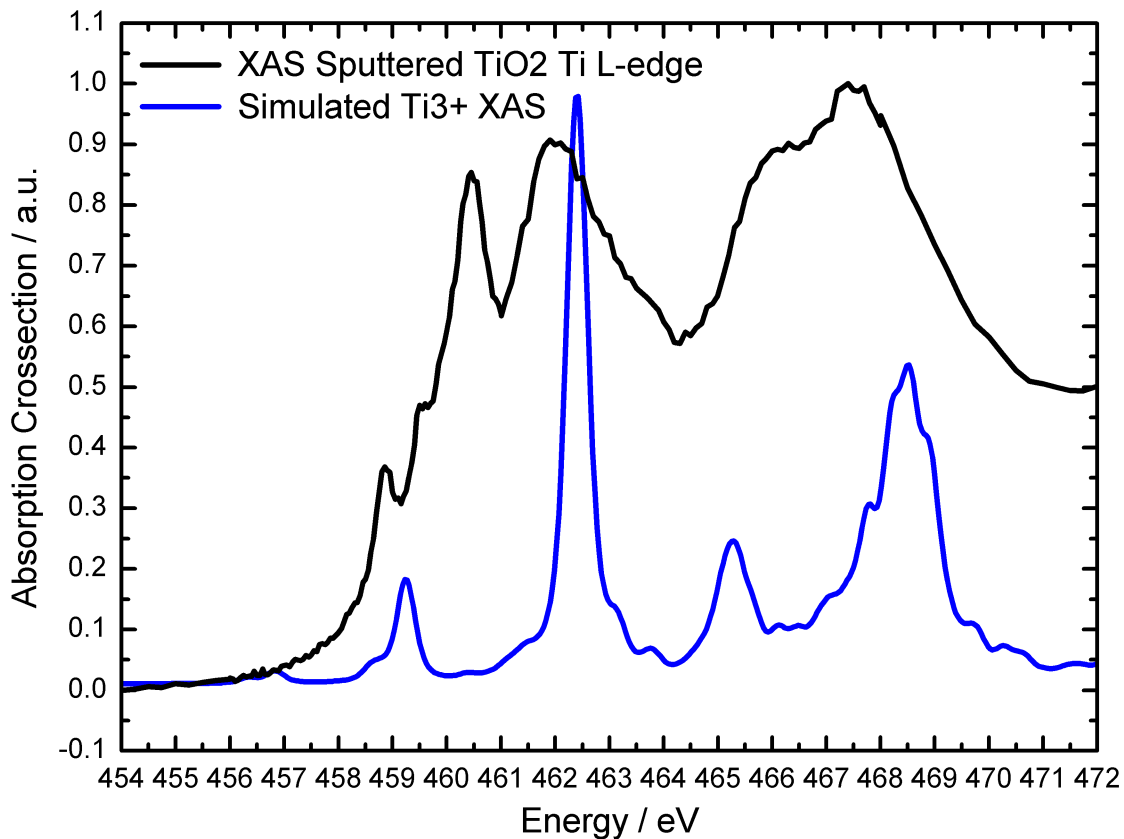


Figure 4.9: The simulated XAS spectrum (in red) of a 2p Ti^{3+} calculation in D_{4h} symmetry with $10 Dq=1.7$ eV, $Ds=0.9$ eV, $Dt=0.8$ eV $\Delta=2.98$ eV, $U_{dd}=4.0$ eV, and $U_{pd}=6.0$ eV, compared against an experimental XAS spectrum (in black) of rutile TiO_2 Ti L -edge. The Lorentzian broadening values used for each peak in the simulated spectrum were 0.1 eV, 0.6 eV, 0.5 eV, and 1.0 eV going from left to right respectively.

The bears very little resemblance to the experimental XAS of the sputtered TiO_2 sample. One could adjust the broadenings, however, I feel even if broadenings were adjusted it would still not adequately describe the experimental spectrum for the sputtered rutile TiO_2 sample. To amend this I feel that TiO_6 values for the crystal field and charge-transfer effects would be more appropriate. As well as this, if oxygen vacancies or surface termination are properly taken into account, then there is no longer a cubic crystal field since one of the ligand oxygens in the cubic octahedron is missing. It is surrounded by only five oxygens in the cubic pyramid arrangement with the Ti in the middle of the square. The local symmetry is then C_{4v} . Therefore, to accurately simulate Ti^{3+} XAS spectra, the point groups symmetry should be reduced to C_{4v} symmetry accordingly.

4.3 Ti^{3+} 2p-3d RIXS

A 2p-3d RIXS multiplet spectrum without charge transfer multiplets was calculated for the Ti^{3+} ion in D_{4h} symmetry. It was simulated using the assumption that it can be described by the same crystal field parameters and point group symmetry used for XAS Ti^{3+} . Figure 4.10 contains the results.

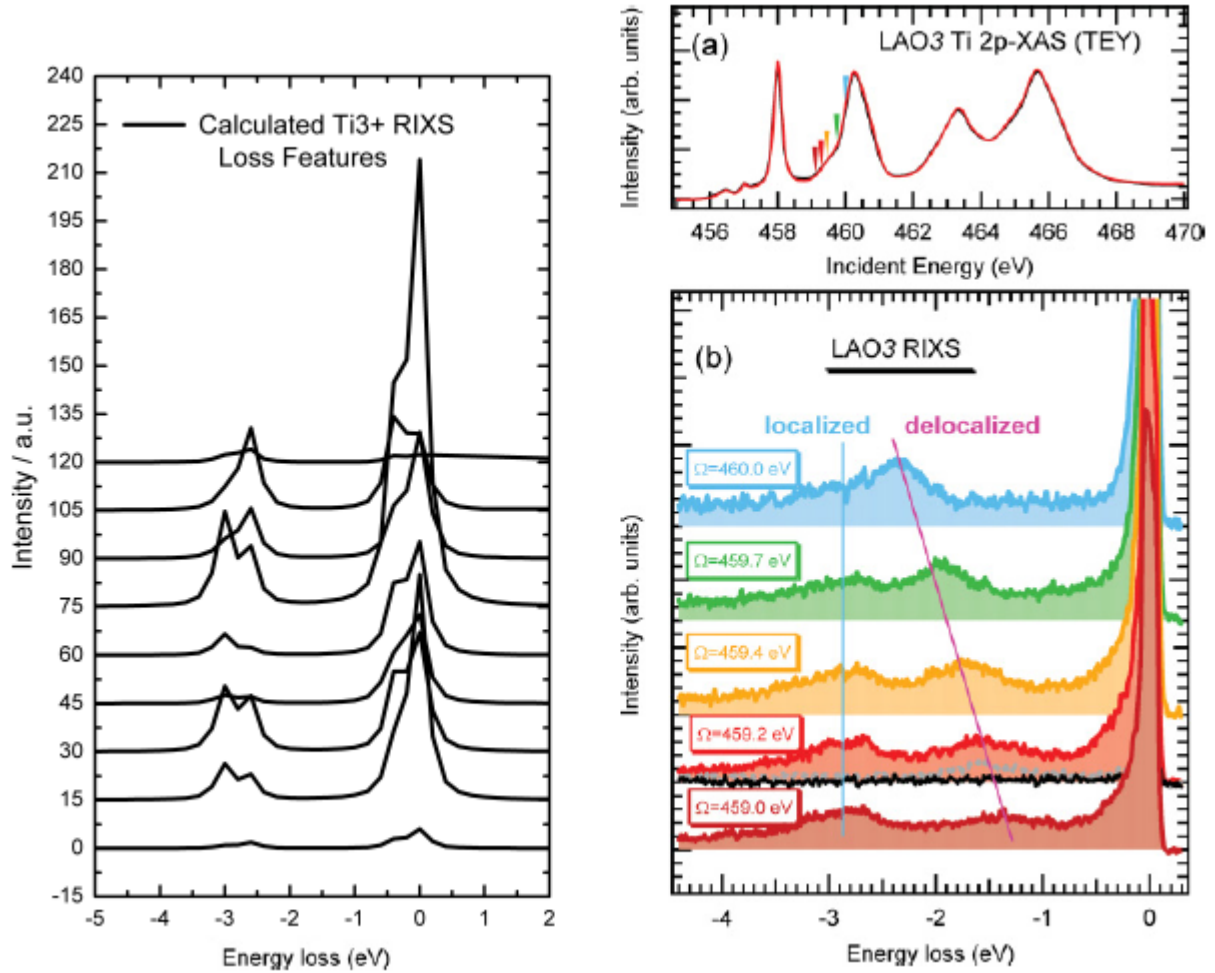


Figure 4.10: The left graph contains a series of calculated RIXS spectra of TiO_2 2p-3d in D_{4h} symmetry with $10 Dq=2.65$ eV, $Ds=-0.1$ eV, $Dt=0.005$ eV taken from [16]. Lorentzian broadenings of 0.4 eV and 0.04 eV were applied. The graphs on the right are experimental data from Ke-Jin Zhou [16]. The top right graph is the total electron yield (TEY) mode 2p-XAS spectra of LAO3 SL for both in-plane (black line) and out-of-plane (red line) polarization. The first two peaks are the Ti^{4+} $2p_{3/2}$ -3d t_{2g} and $2p_{3/2}$ -3d e_g resonances, respectively. Arrows label the incident energies used for RIXS. The lower right graph is a series of RIXS spectra of LAO3 SL excited across the Ti^{3+} $2p_{3/2}$ -3d e_g .

The simulated spectra compare to the experimental spectra quite well. Improvements I would apply if I would be to fine tune the broadenings, lower the point group symmetry to, and calculated the crystal field values from the experimental spectrum itself.

Chapter 5

Conclusions

Although the Ti^{4+} XAS simulations compared quite well against the XAS experimental data of the Ti L -edge TiO_2 sample, a concrete connection was not established between the values of the parameters used in these Ti^{4+} calculations, to the parameters used in the Ti^{3+} calculations. Instead, one needs to obtain separate values for Ti^{3+} simulations to those of the Ti^{4+} . My first, conclusion, would not only be to adjust the point group symmetry to C_{4v} , but, due to how strong the effect of the crystal field parameter $10 Dq$ was on the Ti^{4+} spectrum, investigate the effects of different $10 Dq$ values for Ti^{3+} .

However, in the RIXS simulation of Ti^{3+} , I used crystal field parameters from Ke-Jin Zhou [16]: $Dq=2.65$ eV, $Ds=-0.1$ eV, $Dt=0.005$ eV which compared well to the experimental RIXS Ti^{3+} . In some of the Ti^{4+} calculations in D_{4h} symmetry I used: $10 Dq=2.8$ eV, $Dt=0.0771$ eV, and $Ds=0.1286$ eV. It is interesting to note that there is not a large difference between the $10 Dq$ values, however, not only is there a difference in magnitude between the Dt values, but the Ds values are a different sign to each other. This suggests that the connection between a Ti^{4+} calculation and a Ti^{3+} calculation could be in the values for Ds and Dt .

The RIXS simulation was a good comparison to experiment. However, initially, one had also wanted to include charge-transfer effects. Unfortunately, the CTM4XAS 5.2 software does not as yet allow for charge-transfer effects to be selected during a RIXS calculation and no alternative programs were found. I feel this would be something to compute in the future. As well as repeating the calculation in a lower point group symmetry to replicate the distortions that exist within the Ti^{3+} unit cell.

All in all, the future of spectroscopy appears quite promising. With advances in technology, it is more and more important to understand the surface properties of solids. The transition metal compound TiO_2 itself the subject of many investigations, resulting in advances in technologies such as the memristor. The role of computational methods for simulating spectroscopic experiments, therefore, is only going to grow as it becomes increasingly more necessary to understand entirely the processes of spectroscopic methods.

Appendices

5.1 Appendix A

5.1.1 The Dipole Selection Rules

To a first approximation an XAS spectrum reflects the unoccupied density of states, albeit modified by the selection of conduction band states due to the dipole or quadrupole nature of the transition. To probe the 3d shell 2p, electrons are excited using the x-ray light where the dipole selection rules $\Delta l = \pm 1$, $\Delta j = 0, \pm 1$ allow the transitions [3]:

$$2p_{3/2} \rightarrow 3d_{3/2}, 3d_{5/2}, 4s$$

$$2p_{1/2} \rightarrow 3d_{3/2}, 4s$$

5.1.2 The Hartree-Fock Method

Hartree-Fock (HF) theory is one of the fundamental electronic structure theories. HF theory assumes that the motion of each electron in a system can be described by a single-particle wave function, i.e., no correlations to the instantaneous motion of other electrons of the system are taken into account. It is a good approximation to the actual wave function and thus considered as a useful starting point for more precise calculations.

5.1.3 Larmor Formula

When accelerating or decelerating, any charged particle (such as an electron) radiates away energy in the form of electromagnetic waves. The Larmor formula is used to calculate the total power radiated by a non-relativistic point charge as it accelerates.

$$P = \frac{e^2 a^2}{6\pi\epsilon_0 c^3} (SI\ units) \quad (5.1)$$

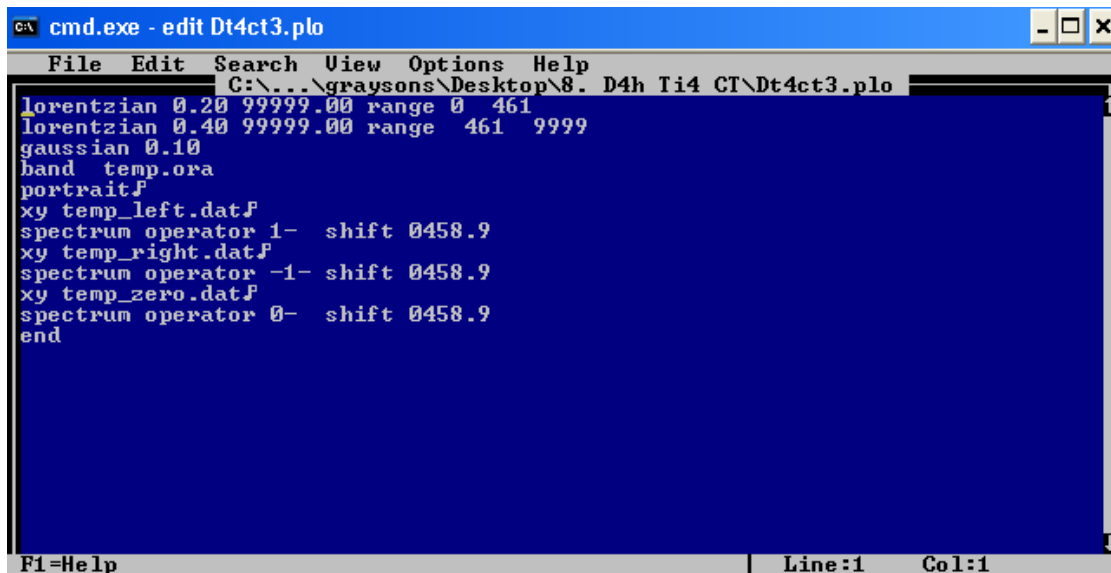
where e is the charge, a is the acceleration, and c is the speed of light.

5.2 Appendix B

5.2.1 Broadening Parameters

Each simulated spectrum within this project has been broadened by lifetime broadening and experimental resolution. From detailed comparison with experiment, it turns out that each of the four main lines has to be broadened differently [3]. However, although the CTM4XAS 5.2 software allows one to define an experimental resolution using a Gaussian broadening, it only allows two lifetime broadenings to be applied. To overcome this limitation, one altered the .plo files produced from the calculation.

To do this, one opened up command prompt and edited the .plo file. Figure 5.1 shows the .plo file before it has been edited. As one can see, only two Lorentzian broadenings have been applied.



```
cmd.exe - edit Dt4ct3.plo
File Edit Search View Options Help
C:\...\graysons\Desktop\8. D4h Ti4 CT\Dt4ct3.plo
lorentzian 0.20 99999.00 range 0 461
lorentzian 0.40 99999.00 range 461 9999
gaussian 0.10
band temp.ora
portrait F
xy temp_left.dat F
spectrum operator 1- shift 0458.9
xy temp_right.dat F
spectrum operator -1- shift 0458.9
xy temp_zero.dat F
spectrum operator 0- shift 0458.9
end
F1=Help | Line:1 Col:1
```

Figure 5.1: The original .plo file containing two Lorentzian and Gaussian broadening parameters.

Thus, one added two more Lorentzian broadening lines stating the additional broadenings and the ranges to which they should apply. Figure 5.2 shows the edited .plo file.

```

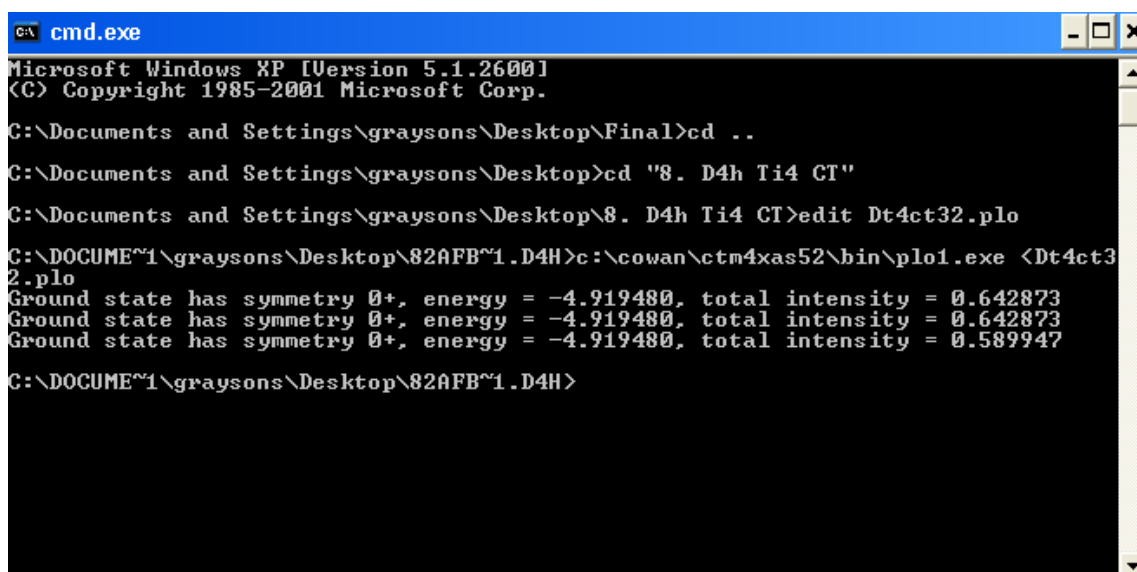
cmd.exe - edit Dt4ct3.plo
File Edit Search View Options Help
C:\...\graysons\Desktop\8. D4h Ti4 CT\Dt4ct3.plo
lorentzian 0.10 99999.00 range 0 458
lorentzian 0.60 99999.00 range 458 461
lorentzian 0.50 99999.00 range 461 464
lorentzian 1.00 99999.00 range 464 9999
gaussian 0.10
band Dt4ct3.ora
portraitF
xy Dt4ct3_left.datF
spectrum operator 1- shift 0458.9
xy Dt4ct3_right.datF
spectrum operator -1- shift 0458.9
xy Dt4ct3_zero.datF
spectrum operator 0- shift 0458.9
end
F1=Help | Line:12 Col:9

```

Figure 5.2: The edited .plo file containing four Lorentzian and one Gaussian broadening parameters.

Other changes which were also made, was the inclusion of the name of the .ora file to which one wanted to apply broadening to. In Figure 5.2 have included this in a yellow box. This is because .ora files are only suitable for calculation not containing charge-transfer effects. If one is editing a calculation for charge-transfer effects this needs to be changed to .oba for the new altered .plo file to work. I also changed the names of the .dat files in the .plo file to the same name as the .ora/.oba file.

Once alterations had been made, the new file was saved and one returned to command prompt. Although the .plo file now contains the new broadenings they have yet to be applied to the calculations. To do this, one ran PLO1.exe with the edited .plo file. Figure 5.3 depicts the action of this.



```
cmd.exe
Microsoft Windows XP [Version 5.1.2600]
(C) Copyright 1985-2001 Microsoft Corp.

C:\Documents and Settings\graysons\Desktop\Final>cd ..
C:\Documents and Settings\graysons\Desktop>cd "8. D4h Ti4 CT"
C:\Documents and Settings\graysons\Desktop\8. D4h Ti4 CT>edit Dt4ct32.plo
C:\DOCUME~1\graysons\Desktop\82AFB~1.D4H>c:\cowan\ctn4xas52\bin\plo1.exe <Dt4ct32.plo
Ground state has symmetry 0+, energy = -4.919480, total intensity = 0.642873
Ground state has symmetry 0+, energy = -4.919480, total intensity = 0.642873
Ground state has symmetry 0+, energy = -4.919480, total intensity = 0.589947
C:\DOCUME~1\graysons\Desktop\82AFB~1.D4H>
```

Figure 5.3: Command prompt running the PLO1.exe for the edited .plo file with the results printed below.

To display the altered spectra, the new .dat files were just imported into Origin and graphed.

CTM4RIXS Paramter Window

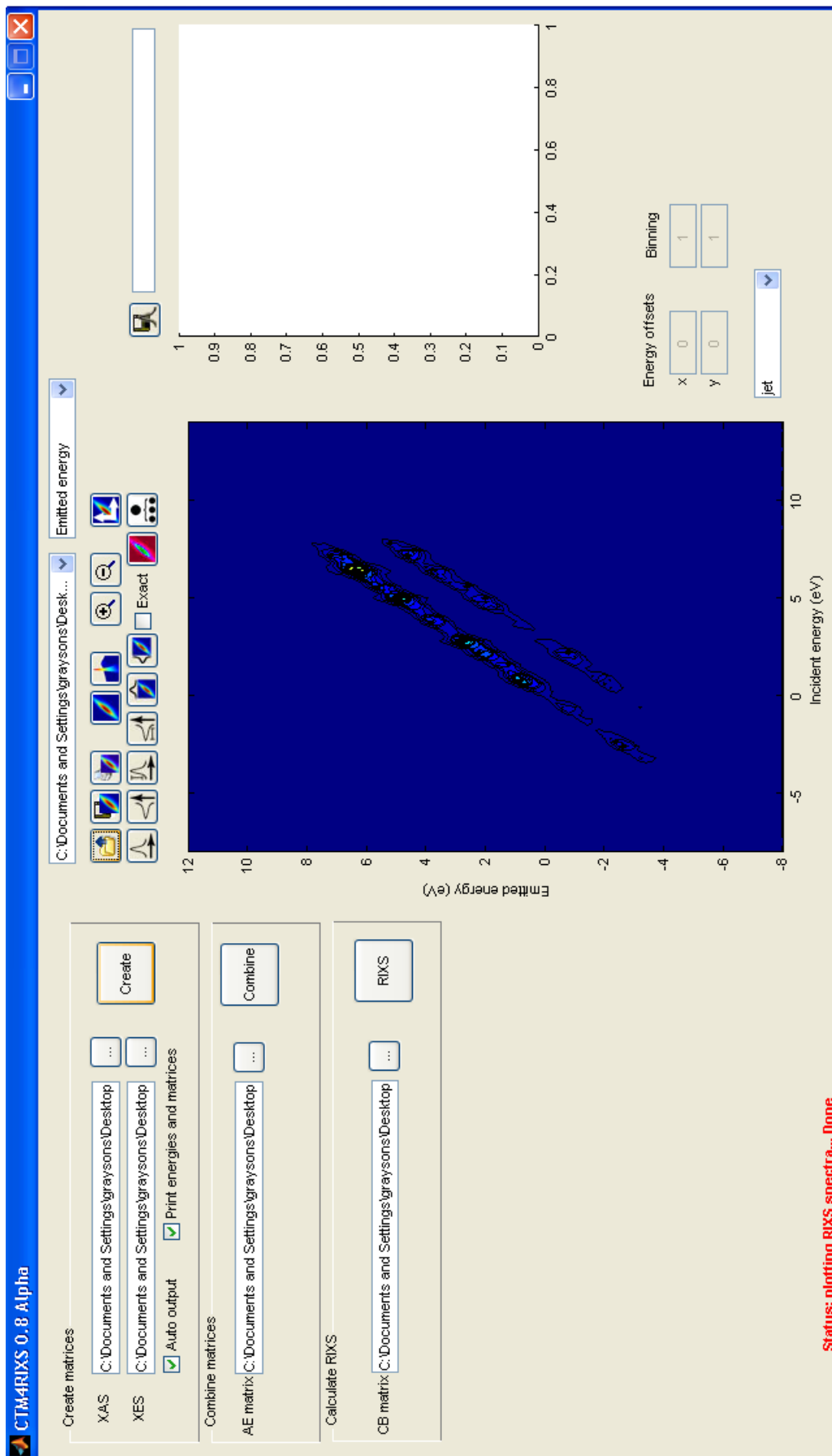


Figure 5.4: CTM4RIXS Parameter Window

5.3 Appendix C

5.3.1 Varying the Crystal Field

As one already mentioned, to find the best value of $10 Dq$ for a Ti^{4+} multiplet calculation in O_h symmetry, one explored how changing the $10 Dq$ value affected the overall shape of the spectrum. The first value to be considered was $10 Dq=0$. I chose this as I wanted to see how the simulated XAS spectrum of the Ti^{4+} calculation appeared before any crystal field affects were included. Figure 5. shows the result.

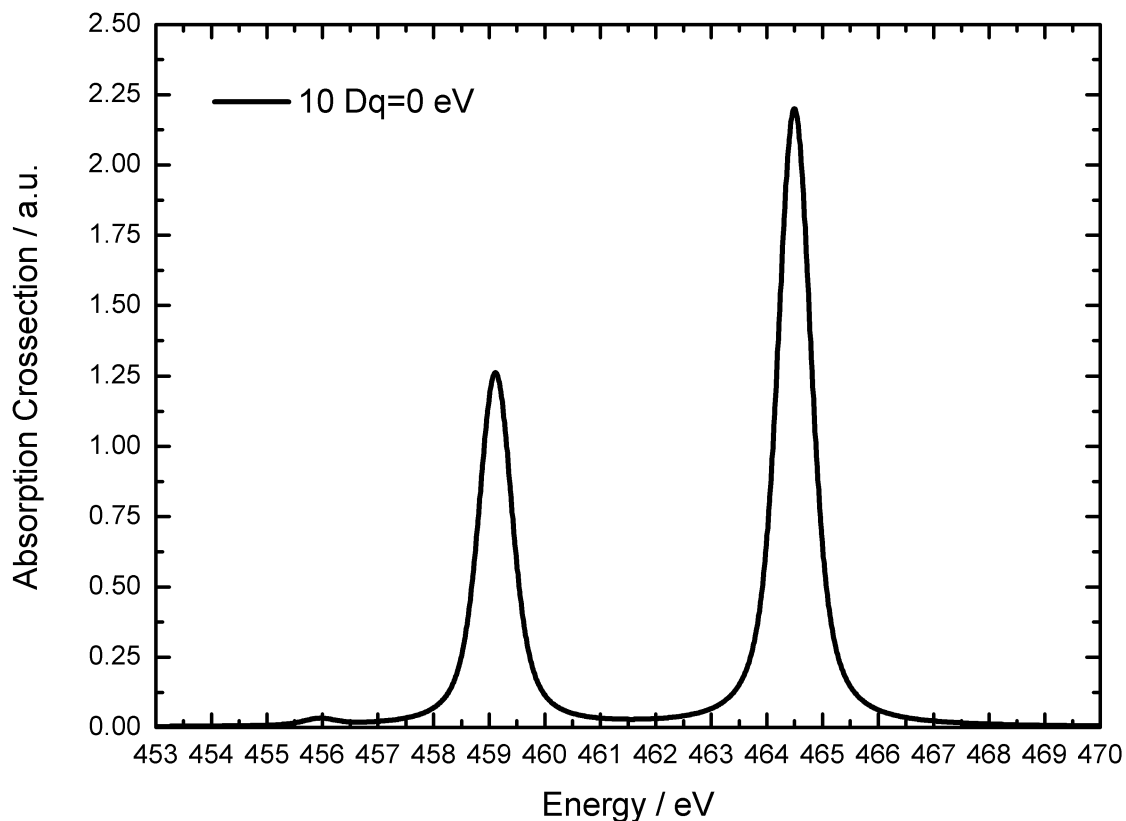


Figure 5.5: The simulated XAS spectrum of a 2p Ti^{4+} calculation in O_h symmetry with $10 Dq=0$ eV.

Only the L_3 and L_2 features are present, respectively. This is to be expected as in octahedral symmetry, $10 Dq$ is defined as the energy difference between the t_{eg} states and the e_g states, neglecting all atomic parameters.

$10 Dq$ was then varied between -2.0 eV and $+2.0$ eV in steps of 0.4 eV, to see how negative values compare against positive values.

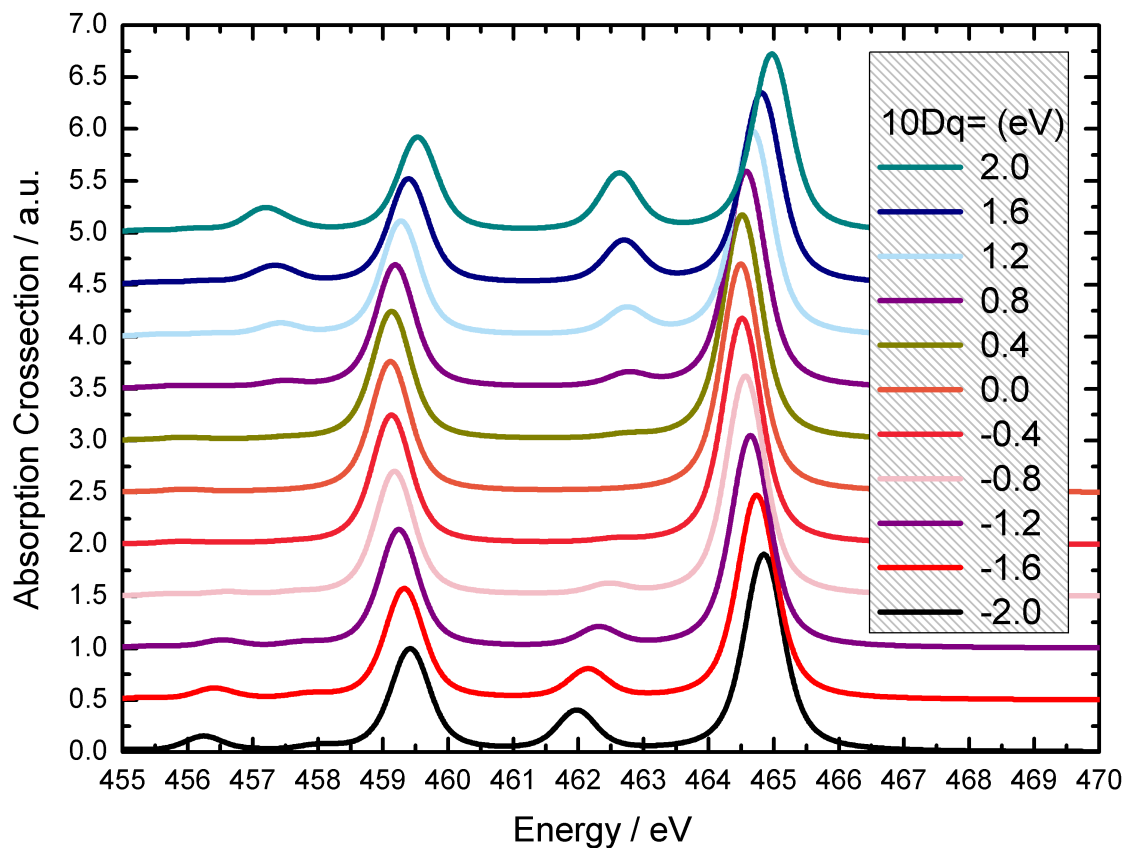


Figure 5.6: The simulated XAS spectrum of a 2p Ti⁴⁺ calculation in O_h symmetry with 10 Dq varied between -2.0 eV and +2.0 eV in steps of 0.4 eV.

The main difference appears to be the slight shift of the L_3 and $L_2 t_{2g}$ states of the negative calculations to the left. Creating a smaller separation between the L_3 and L_2 features. Although, the difference is quite small, from consulting values used within similar calculations contained in the literature pertaining to TiO₂, a positive 10 Dq value appears to be the best match. I therefore calculated spectra with 10 Dq varying between 1 eV and 3 eV in steps of 0.25 eV. Figure 5. shows the results.

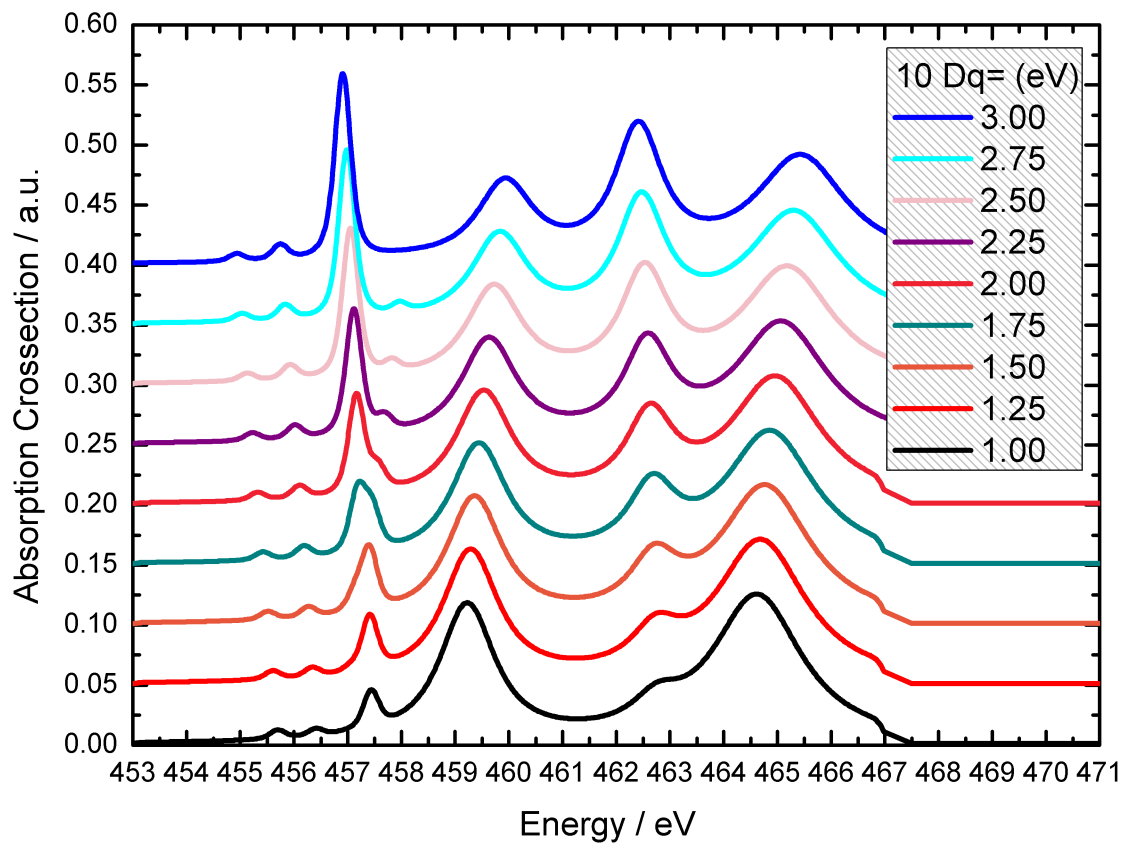


Figure 5.7: The simulated XAS spectrum of a $2p$ Ti^{4+} calculation in O_h symmetry with $10 Dq$ varied between 1.0 eV and 3.0 eV in steps of 0.25 eV.

Continuing this process, one eventually decided upon a value of $10 Dq=1.8$ eV, as this appeared to replicate the crystal field found in experimental XAS TiO_2 Ti L -edge spectra the best.

5.3.2 Crystal Field Parameters

For calculations involving more than just the 10 Dq crystal field value, i.e., D_{4h} symmetry calculations, I deducted 10 Dq, Dt, and Ds from Declan's experimental spectra of TiO₂ rutile Ti *L*-edge.

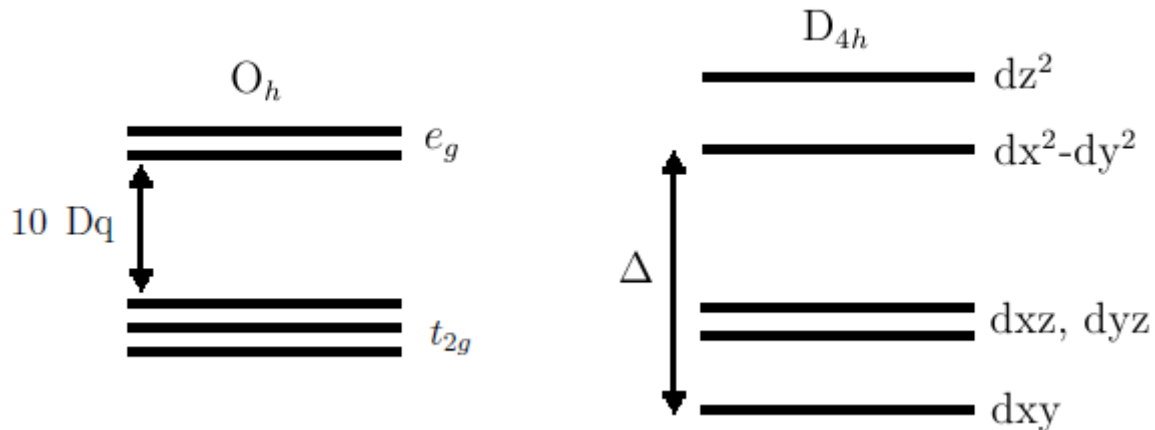


Figure 5.8: The energy splitting of O_h symmetry and D_{4h} symmetry.

From Figure 5 :

$$\Delta = (dx^2 - y^2) - (dxy) \quad (5.2)$$

$$= 10Dq \quad (5.3)$$

From Table 2.1 :

$$(dxy, dyz) - (dxy) = (-4Dq - 1Ds + 4Dt) - (-4Dq + 2Ds - 1Dt) \quad (5.4)$$

$$= -3Ds + 5Dt \quad (5.5)$$

and

$$(dx^2 - y^2) - (dz^2) = (6Dq + 2Ds - 1Dt) - (6Dq - 2Ds - 6Dt) \quad (5.6)$$

$$= 4Ds + 5Dt \quad (5.7)$$

Assuming there is no degeneracy of the dxy, dyz, and dxz states, one sets $-3Ds + 5Dt = 0$. However, there appears to be a slight splitting of the L_3 e_g peak in the experimental Ti *L*-edge XAS. The higher energy peak corresponds to dz^2 and the lower to $dx^2 - y^2$. Thus, by determining the difference in energy between these two peaks from

the spectrum's graph I equated $4D_s + 5D_t = 0.9eV$. Values for D_s and D_t were then found by simultaneous equations.

$$-3D_s + 5D_t = 0eV \quad (5.8)$$

$$4D_s + 5D_t = 0.9eV \quad (5.9)$$

$$-7D_s = 0.9eV \quad (5.10)$$

$$D_s = -0.9eV/7 \quad (5.11)$$

$$D_s = -0.1286 \quad (5.12)$$

The value for D_s was then substituted into $-3D_s + 5D_t = 0eV$ and D_t was found to be $D_t = -0.0771$ eV. The 10 D_q values was also measured from the spectrum and found to be $10 D_q = 2.8$ eV.

5.3.3 RIXS Simulation: Incident Energy Vs Emitted Energy

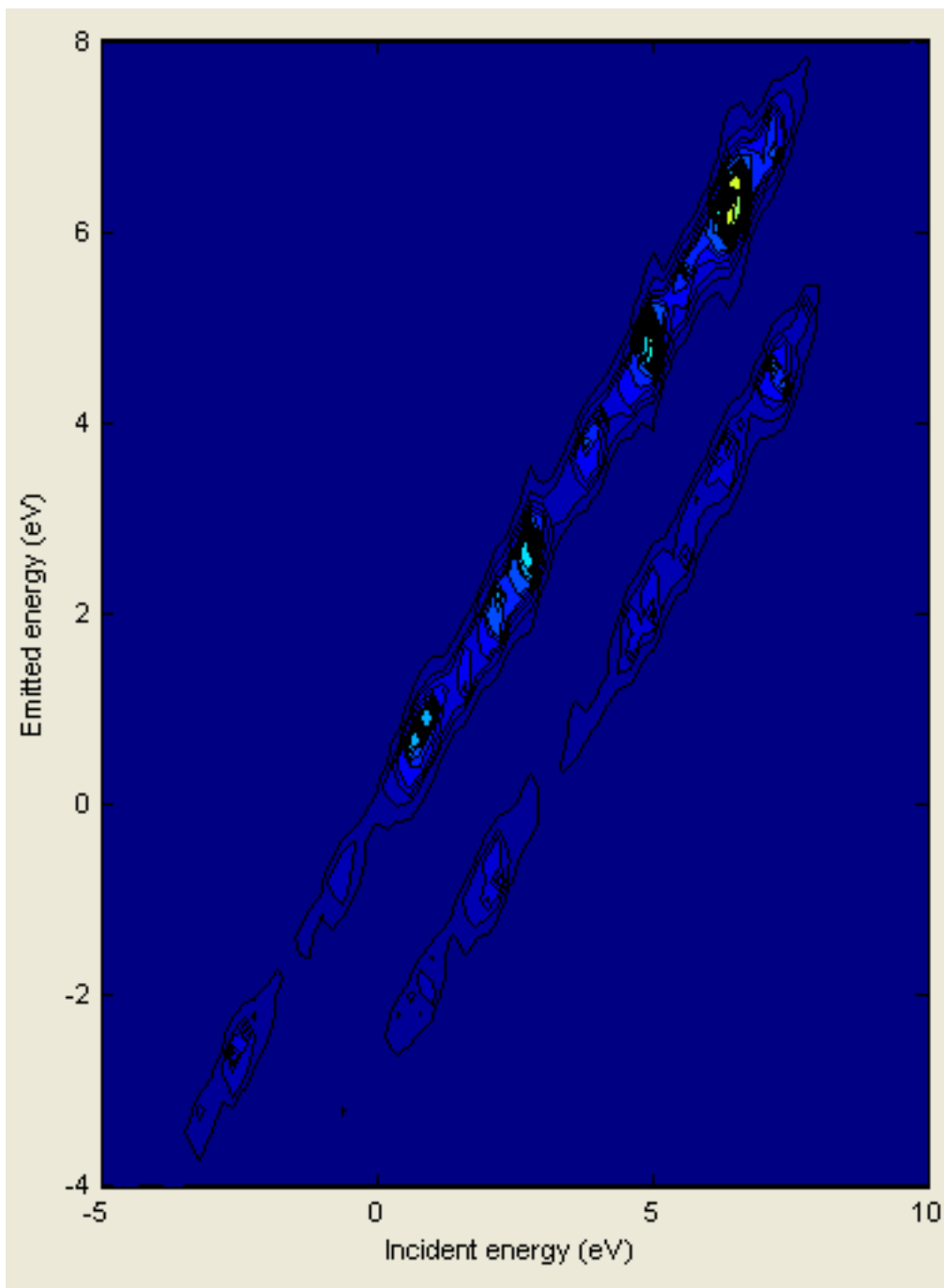


Figure 5.9: RIXS Simulation Calculation Incident Energy Versus Emitted Energy Plot.

Bibliography

- [1] Akio Kotani and Shik Shin “Resonant Inelastic X-Ray Scattering Spectra for Electrons in Solids”, Rev. Mod. Phys. 73, (2001), pp. 203-242.
- [2] Declan Cockburn, “Electronic Structure, Bonding and Dichroism in Rutile Compounds. An X-Ray Spectroscopy Study.”, Phd Thesis, Trinity College Dublin, (2012)
- [3] Frank de Groot and Akio Kotani, *Core Level Spectroscopy of Solids*, Vol. 6, CRC Press, (2008).
- [4] Sanjukta Choudhury, “Spectroscopic Study of Transition Metal Compounds”, Phd Thesis, University of Saskatchewan, (2010).
- [5] Brendan James Arnold, “Growth and Characterisation of Al(Cr)N thin films by r.f. Plasma Assisted Pulsed Laser Deposition”, Msc Thesis, Trinity College Dublin, (2009).
- [6] R. P. Feynman, F. B. Moringo, and W. G. Wagner, *Feynman Lectures on Gravitation*, Addison-Wesley, (1995).
- [7] Anne P. Thorne, Ulf Litzan, Sveneric Johansson, *Spectrophysics: Principles and Applications*, Springer,
- [8] F. M. F. de Groot and J. C. Fuggle, “ $L_{2,3}$ x-ray-absorption edges of d^0 compounds: K^+ , Ca^{2+} , Sc^{3+} , and Ti^{4+} in O_h (octahedral) symmetry”, Phys. Rev. B 41, (1990), pp. 928-937.
- [9] Milton Orchin, Roger S. Macomber, Allan Pinhas, Marshall R. Wilson, *Atomic Orbital Theory*, (2005).
- [10] Darl H. McDaniel, “Spin Factoring as an Aid in the Determination of Spectroscopic Terms”, J Chem. Edu. 54, 3, (1977), p. 147.
- [11] E. Stavitski and F.M.F. de Groot, “The CTM4XAS program for EELS and XAS spectral shape analysis of transition metal L -edges” Micron 41, (2010), pp. 687-694.
- [12] Russell S. Drago, *Physical Methods in Chemistry*, W.B. Saunders Company, (1977).

- [13] Martin S. Silberberg, *Chemistry: The Molecular Nature of Matter and Change*, 4th Ed, New York: McGraw Hill Company, (2006).
- [14] Eli Stavitski and Frank de Groot, *CTM4XAS 5.2 Manual*, Version 1, (2008).
- [15] Stephan Callaghan, Personal correspondence.
- [16] Ke-Jin Zhou, Milan Radovic, Justine Schlappa, Vladimir Strocov, Ruggero Frison, Joel Mesot, Luc Patthey, and Thorsten Schmitt, “Localized and delocalized Ti 3d carriers in LaAlO₃/SrTiO₃ superlattices revealed by resonant inelastic x-ray scattering”, *Phy. Rev. B*, 83, (2011), pp. 201402-1.
- [17] Masahiko Matsubara, Takayuki Uozumi, Akio Kotani, Yoshihisa Harada and Shik Shin, “Polarization Dependence of Resonant X-Ray Emission Spectra in Early Transition Metal Compounds”, *J. Phys. Soc. of Japan*, 69, 5, (2000), pp. 1558-1565.